World Journal of Diabetes

Submit a Manuscript: https://www.f6publishing.com

World J Diabetes 2025 October 15; 16(10): 109568

DOI: 10.4239/wjd.v16.i10.109568

ISSN 1948-9358 (online)

ORIGINAL ARTICLE

Basic Study

Nephroprotective mechanism of Kunkui Baoshen decoction in diabetic kidney disease: Targeting the HERC2/NCOA4-mediated autophagy-dependent ferroptosis pathway

Si-Yuan Song, Chu-Chu Shan, Pei-Pei Zhou, Wei-Long Xu, Ying Tan, Xi-Qiao Zhou, Li-Ji Huang, Qian-Hua Yan, Jiang-Yi Yu

Specialty type: Endocrinology and metabolism

Provenance and peer review: Unsolicited article; Externally peer reviewed.

Peer-review model: Single blind

Peer-review report's classification

Scientific Quality: Grade B, Grade B, Grade B, Grade B

Novelty: Grade B, Grade B, Grade C

Creativity or Innovation: Grade B, Grade B, Grade C

Scientific Significance: Grade A, Grade B, Grade C

P-Reviewer: Baddam S, MD, United States; Horowitz M, DSc, MD, PhD, FRACP, Professor, Australia; M. Hussein A, PhD, Associate Professor, Senior Researcher, Iraq; Wang P, Chief Physician, Professor, China

Received: May 15, 2025

Revised: June 3, 2025

Accepted: August 15, 2025

Published online: October 15, 2025

Processing time: 153 Days and 19.2 Hours

Si-Yuan Song, Chu-Chu Shan, Pei-Pei Zhou, Wei-Long Xu, Ying Tan, Xi-Qiao Zhou, Li-Ji Huang, Qian-Hua Yan, Jiang-Yi Yu, Department of Endocrinology, Jiangsu Province Hospital of Chinese Medicine, Affiliated Hospital of Nanjing University of Chinese Medicine, Nanjing 210000, Jiangsu Province, China

Co-first authors: Si-Yuan Song and Chu-Chu Shan.

Co-corresponding authors: Qian-Hua Yan and Jiang-Yi Yu.

Corresponding author: Jiang-Yi Yu, MD, Department of Endocrinology, Jiangsu Province Hospital of Chinese Medicine, Affiliated Hospital of Nanjing University of Chinese Medicine, No. 155 Hanzhong Road, Qinhuai District, Nanjing 210000, Jiangsu Province, China. 1401743118@qq.com

Abstract

BACKGROUND

Diabetic kidney disease (DKD) stands as the key contributor to chronic kidney disease worldwide. Clinical studies have shown that Kunkui Baoshen decoction (KKBS) effectively reduces proteinuria and enhances renal function in DKD patients. However, its precise molecular targets and therapeutic mechanisms remain to be thoroughly clarified.

AIM

To evaluate the nephroprotective efficacy of KKBS in DKD and explore the underlying mechanisms of action.

METHODS

Liquid chromatography-tandem mass spectrometry was utilized to analyze the chemical constituents of KKBS. Metabonomic and transcriptomic analyses were conducted to identify key targets and pathways associated with the therapeutic effects of KKBS on DKD. The nephroprotective effects of KKBS were assessed both in high glucose-induced human kidney-2 cells and in db/db mice. A variety of assays were performed, including Cell Counting Kit-8, Western blot, quantitative reverse transcription-polymerase chain reaction, immunofluorescence, co-immunoprecipitation, periodic acid-Schiff staining, Masson staining, hematoxylin

and eosin staining, immunohistochemistry, and mitochondrial morphology analysis.

RESULTS

The glutathione metabolic pathway emerged as the most prominent metabolic pathway in the metabonomic analysis of KKBS. Transcriptomic and bioinformatic analyses revealed that nuclear receptor coactivator 4 (NCOA4) was instrumental in regulating ferroptosis within renal tubules of mice with DKD. Both *in vitro* and *in vivo* experiments showed that KKBS ameliorated renal dysfunction, mitigated renal tissue damage, and repressed the expression of autophagy-dependent ferroptosis markers and inflammatory fibrosis. Mechanistically, KKBS enhanced the interaction between the homologous to E6-AP C-terminus and RCC1-like domain-containing E3 ubiquitin protein ligase (HERC2) and NCOA4, leading to K48-related ubiquitination and subsequent degradation of NCOA4. This process inhibited autophagy-dependent ferroptosis, reduced the release of pro-fibrotic inflammatory factors, and ultimately exerted an anti-fibrotic effect in DKD.

CONCLUSION

KKBS confers nephroprotection in DKD by modulating HERC2/NCOA4-mediated autophagy-dependent ferroptosis, thereby alleviating renal fibrosis.

Key Words: Ubiquitination; Ferroptosis; Diabetic kidney disease; Renal fibrosis; Kunkui Baoshen decoction

©The Author(s) 2025. Published by Baishideng Publishing Group Inc. All rights reserved.

Core Tip: Kunkui Baoshen decoction (KKBS), a traditional Chinese herbal formula, exerts renoprotective effects in diabetic kidney disease (DKD) by inhibiting autophagy-dependent ferroptosis. Through integrated transcriptomic and metabolomic analyses, we identified the homologous to E6-AP C-terminus and RCC1-like domain-containing E3 ubiquitin protein ligase/nuclear receptor coactivator 4 axis as a critical therapeutic target. KKBS enhances homologous to E6-AP C-terminus and RCC1-like domain-containing E3 ubiquitin protein ligase-mediated K48-linked ubiquitination of nuclear receptor coactivator 4, promoting its degradation and thereby suppressing ferroptosis, renal inflammation, and fibrosis in high glucose-induced human kidney-2 cells and db/db mice. This research reveals a novel pathway through which KKBS regulates ferroptosis to prevent DKD progression.

Citation: Song SY, Shan CC, Zhou PP, Xu WL, Tan Y, Zhou XQ, Huang LJ, Yan QH, Yu JY. Nephroprotective mechanism of Kunkui Baoshen decoction in diabetic kidney disease: Targeting the HERC2/NCOA4-mediated autophagy-dependent ferroptosis pathway. *World J Diabetes* 2025; 16(10): 109568

URL: https://www.wjgnet.com/1948-9358/full/v16/i10/109568.htm

DOI: https://dx.doi.org/10.4239/wjd.v16.i10.109568

INTRODUCTION

Diabetic kidney disease (DKD) continues to be the predominant driver of chronic kidney disease, accounting for nearly 50% of chronic kidney disease cases globally[1]. Although therapies such as sodium-glucose cotransporter-2 inhibitors, renin-angiotensin system inhibitors, and newer mineralocorticoid receptor antagonists have demonstrated efficacy in reducing adverse renal outcomes and are widely recommended in clinical guidelines[2], the global incidence of DKD continues to rise alarmingly, with many cases progressing to end-stage kidney disease[3].

According to 2023 data from the China National Renal Data System, DKD now accounts for 29.9% of newly initiated hemodialysis cases in China, surpassing primary glomerular diseases (28.7%) for the first time[4]. These statistics highlight an urgent need to enhance DKD prevention and treatment. In this context, it is critical to provide deeper insight into the underlying molecular mechanisms of DKD and to develop

innovative therapeutic strategies that can effectively manage its progression.

Traditional Chinese medicine (TCM) is broadly utilized for DKD treatment in China. KKBS, formulated by Song and Yu[5], two renowned TCM practitioners from Jiangsu Province, is a clinically established herbal prescription composed of *Astragali Radix*, *Abelmoschi Corolla*, *Tripterygium hypoglaucum* root, and *Corni Fructus Preparata*. The formula is derived from Jisheng Shenqi Wan, itself rooted in Jisheng Fang, a prescription widely used during the Southern Song Dynasty. Traditionally, KKBS has been used to warm the kidney, regulate qi, promote diuresis, and alleviate edema. Its clinical indications include kidney deficiency syndromes characterized by edema and soreness in the lower back and knees.

Modern pharmacological research has validated the multifaceted therapeutic potential of KKBS. *Abelmoschi Corolla* alleviates DKD-related proteinuria and renal injury by reducing tubular damage and interstitial fibrosis, oxidative stress, inflammatory responses, and podocyte apoptosis[6]. *Tripterygium hypoglaucum* root improves renal function by protecting glomerular endothelial cells, suppressing inflammatory factor expression, enhancing immunosuppression, and reducing proteinuria and hematuria[7]. *Astragali Radix* has been demonstrated to lower blood glucose levels, reduce proteinuria, and exert nephroprotective effects in DKD animal models[8]. The main active compound in *Corni Fructus Preparata*, loganin, mitigates inflammation and organelle damage in DKD cell models by inhibiting advanced glycation end product-triggered oxidative stress, suppressing mesangial cell proliferation, and alleviating endoplasmic reticulum stress [9]. Clinical research has additionally demonstrated that KKBS effectively reduces proteinuria and maintains kidney function in patients with DKD[5]. However, the specific molecular targets and mechanisms through which KKBS exerts its therapeutic effects remain uncertain.

Ferroptosis is a controlled type of cell death reliant on iron, marked by the buildup of reactive oxygen species (ROS) and the polyunsaturated fatty acids' depletion in cellular membranes[10]. This process is mediated by complex molecular pathways, including those related to iron[11], lipid[12], and amino acid metabolism[13], along with signaling pathways associated with coenzyme Q[14], p53[15], inositol trisphosphate 3-kinase[16], and mitochondrial voltage-dependent anion channels[17]. In terms of morphology, ferroptosis is marked by mitochondrial shrinkage or swelling, raised membrane density, and a loss of cristae, distinctive features differentiating it from other cell death types[18]. An increasing volume of evidence implicates ferroptosis in the pathogenesis of DKD[19,20], suggesting that targeting this process may reduce renal fibrosis and slow disease progression.

To examine the anti-fibrotic mechanism of KKBS in DKD, we conducted metabolomic analysis to identify its relevant metabolic pathways. Glutathione (GSH) metabolism emerged as the most significantly altered pathway following KKBS treatment. Given the pivotal role of GSH homeostasis in regulating ferroptosis, these results suggest that KKBS may exert its nephroprotective impact by modulating ferroptosis. Building on this hypothesis, both *in vitro* and *in vivo* experiments were performed utilizing high glucose (HG)-induced human kidney-2 (HK-2) cells and db/db mice to investigate the impact of KKBS on ferroptosis in DKD. Our findings may offer a novel therapeutic approach for alleviating renal injury in DKD.

MATERIALS AND METHODS

Analysis of KKBS components and metabonomics analysis

The four Chinese herbal medicine used in the KKBS (Table 1) were sourced from Jiangsu Province Hospital of Chinese Medicine, Nanjing, China.

Preparation and liquid chromatography-tandem mass spectrometry analysis of KKBS: Following the original formulation and adjustment for contemporary clinical dosages, the preparation of KKBS involved the precise weighing and mixing of four herbal components: *Astragali Radix* (30 g), *Tripterygium hypoglaucum* root (15 g), *Corni Fructus Preparata* (10 g), and *Abelmoschi Corolla* (30 g). The mixture was soaked in water for 30 minutes and then decocted twice, first with 10 times the volume of water for 30 minutes, followed by a second decoction using 8 times the volume, also for 30 minutes. The combined extracts were then condensed to a final volume of 170 mL, resulting in a solution concentration of 1 g/mL. In accordance with established everted rat gut sac protocols[21], the final KKBS preparation was stored at 4 °C. Quality control measures were implemented to ensure the reproducibility of the KKBS solution, and liquid chromatography-tandem mass spectrometry (LC-MS/MS)[22] was applied for quality assurance and chemical profiling.

Metabonomics analysis: To clarify the metabolic pathways influenced by KKBS in DKD, differential metabolites were analyzed in plasma samples from untreated db/db mice compared to those treated with KKBS. The raw LC-MS data underwent processing with Progenesis QI software (Waters Corporation, Milford, MA, United States), which included baseline correction, peak detection, data alignment, and retention time calibration. This yielded a data matrix consisting of retention time, mass-to-charge ratio, and intensity values. Metabolite identification was conducted by spectral matching against the HMDB (http://www.hmdb.ca/)[23], METLIN (https://metlin.scripps.edu/)[24], and Meiji's in-house database. The annotated dataset was subsequently uploaded to the Meiji Cloud Platform (cloud.majorbio.com) for further bioinformatics analysis[25]. Data preprocessing followed a systematic approach: Variables with more than 20% missing values were excluded based on the 80% rule, ensuring retention of variables with non-zero values in at least 80% of samples in one group. Missing data were imputed using the minimum observed values from the original dataset to account for variability due to sample handling and instrument performance. Total ion current normalization was applied to correct for technical variation in mass spectrometry signal intensity. Finally, features with a relative standard deviation > 30% in quality control samples were filtered out to increase data robustness.

The remaining data were transformed using log10 conversion to stabilize variance and normalize the distribution for downstream analyses. Multivariate statistical analysis was conducted utilizing the ropls package (version 1.6.2), where principal component analysis and orthogonal projections to latent structures-discriminant analysis models were assessed through 7-fold cross-validation. Metabolite significance was assessed based on variable importance in projection scores obtained from the orthogonal projections to latent structures-discriminant analysis model as follows:

$$VIP_j = \sqrt{\frac{p}{\sum_{h=1}^{H} SS(h)}} \cdot \sum_{h=1}^{H} w_{jh}^2 \cdot SS(h)$$

where P represents the total number of metabolites, H denotes the number of principal components included in the model, W_{jh} refers to the weight of the j^{th} metabolite in the h^{th} principal component, and $SS(h)$ indicates the sum of squares of the h^{th} principal component.

A two-tailed hypothesis test was applied, and the false discovery rate correction was used to adjust for multiple comparisons. Statistical significance was set utilizing Student's t-test ($P < 0.05$) in combination with variable importance in projection scores > 1. Pathway enrichment analysis was performed utilizing the Kyoto Encyclopedia of Genes and Genomes (KEGG) database (https://www.kegg.jp/kegg/pathway.html)[26], and pathway relevance was evaluated using Fisher's exact test, implemented *via* the scipy.stats module in Python.

Molecular docking: Compound structures were retrieved from PubChem (https://pubchem.ncbi.nlm.nih.gov/), and corresponding protein targets were obtained from the PDB database (https://www.rcsb.org/)[27]. Protein preparation was performed using AutoDock 4.2.6, which included the elimination of water molecules, incorporation of hydrogen atoms, and allocation of partial charges, followed by conversion of the structures to the PDBQT format. Molecular docking simulations were performed with AutoDock Vina version 1.1.2[28], and the docking outcomes were visualized with PyMOL 2.3.0.

Transcriptomic analysis

RNA isolation: Total RNA was extracted from renal tissues of the db/db group and the KKBS treatment group ($n = 3$ per group; detailed grouping information is available in section 2.3.9.1) using TRIzol® reagent (Magen, Guangzhou, China). RNA purity and integrity were assessed utilizing a Nanodrop ND-2000 (Thermo Scientific, MA, United States) for A260/280 ratios and the Agilent 4150 Bioanalyzer (RIN evaluation). Only samples meeting quality criteria proceeded to library construction.

Library preparation and sequencing: Paired-end libraries were constructed following standard protocols using the mRNA-seq Library Prep Kit (ABclonal, Wuhan, China). Shortly, 1 μg of total RNA was subjected to poly(A)+ RNA enrichment utilizing oligo(dT) magnetic beads. Moreover, fragmentation was performed with ABclonal's proprietary cation-containing buffer under elevated temperatures. First-strand complementary DNA was produced utilizing random hexamer primers and an RNase H-active reverse transcriptase, which was then followed by second-strand synthesis employing DNA polymerase I and RNase H. Sequencing adapters were attached to the resulting double-stranded complementary DNA fragments. Indexed libraries were amplified and size-selected using AMPure XP beads. Library quality was validated *via* electrophoretic analysis on the Agilent 4150 system before sequencing on either the Illumina NovaSeq 6000 or the MGI MGISEQ-T7 platform.

Data analysis: Raw sequencing data were analyzed utilizing the DESeq2 package (http://bioconductor.org/packages/release/bioc/html/DESeq2.html)[29] to identify differentially expressed genes (DEGs). Genes with $|\log_2 \text{fold change}| > 1$ and $P < 0.05$ were deemed statistically significant. Moreover, DEGs' functional enrichment analysis was performed using the KEGG database. Gene Ontology and KEGG pathway enrichment analyses were carried out utilizing the clusterProfiler package in R, with Benjamini-Hochberg adjusted P value < 0.05 supposed statistically significant[30].

For integrative pathway analysis, we utilized the "Joint Pathway Analysis" module in MetaboAnalyst 5.0, which combines transcriptomic and metabolomic data by mapping DEGs and metabolites onto KEGG pathways. Enrichment was determined using a hypergeometric test followed by false discovery rate correction, with pathways meeting an adjusted P value < 0.05 considered significantly enriched.

Experimental analysis in vivo and in vitro

Culturing conditions: HK-2 cells were obtained from Wuhan Procell Life Science and Technology Co., Ltd. (CL-0109, Wuhan, China) in March 2024. Cells were cultured in low-glucose Dulbecco's modified Eagle medium/F12 medium enriched with 10% foetal bovine serum (PM150312B, Procell, Wuhan, China) at 37 °C in a humidified atmosphere comprising 5% CO_2. The experimental groups and treatment conditions were as follows: Normal glucose group: 5.5 mmol/L glucose; HG group: 50 mmol/L glucose to simulate diabetic conditions; mannitol group: 50 mmol/L mannitol to control for osmotic effects; HG + KKBS group: 50 mmol/L glucose with 14% KKBS; HG + ferrostatin-1 (Fer-1) group: 50 mmol/L glucose with 10 μM Fer-1; HG + Fer-1 + KKBS group: 50 mmol/L glucose with 10 μM Fer-1 and 14% KKBS. When HK-2 cells reached approximately 95% confluence, treatments were applied and maintained for 24 hours.

Research resource identifier: Authentication of the HK-2 cell line was conducted *via* short tandem repeat profiling, yielding a match score exceeding 90% compared to the American Type Culture Collection reference profile. This confirmed the identity of the cell line and ruled out misidentification or cross-contamination. Short tandem repeat profiling was conducted by Wuhan Procell Life Science and Technology Co., Ltd. Additionally, all cell cultures were routinely screened for mycoplasma contamination prior to experimentation utilizing the MycoAlert™ Mycoplasma Detection Kit (Lonza, MD, United States). All tests returned negative results, confirming that the cell lines used in the

experiments were free from mycoplasma contamination.

Cell proliferation analysis: Cellular proliferative capability was evaluated utilizing the Cell Counting Kit-8 (CCK-8) colorimetric assay kit (C0037, Beyotime Biotechnology, Shanghai, China). After 24 hours of KKBS treatment, cells were treated with 10% CCK-8 reagent and incubated at 37 °C for 2 to 4 hours. Following incubation, optical density was estimated at 450 nm utilizing a microplate spectrophotometer.

Fe^{2+}/Fe^{3+}, malondialdehyde, ROS, and reduced/oxidized GSH analysis: Intracellular and tissue levels of Fe^{2+}/Fe^{3+} and malondialdehyde (MDA; A039-2-1 and A003-1-2, respectively; Nanjing Jiancheng Bioengineering Institute, Nanjing, China) and reduced/oxidized GSH (GSH/GSSG) and ROS (S0053 and S0033S, respectively; Beyotime Biotechnology, Shanghai, China) were quantified according to the manufacturers' protocols.

Scratch assay: Cells were plated in 6-well plates and maintained in culture until approximately 95% confluence. Additionally, a straight-line scratch was made utilizing a 200 μL pipette tip. Furthermore, the wells were rinsed with phosphate buffered saline (C0221A, Beyotime Biotechnology, Shanghai, China) to eliminate detached cells. Complete medium (2 mL per well) was added, and images of the initial wound (0 hour) were captured using an inverted microscope. After 24 hours, images were taken at the same locations. Migration rates were calculated as: [(Wound width at 0 hour - width at 24 hours)/0 hour width] × 100%.

Quantitative reverse transcription-polymerase chain reaction: Total RNA was isolated using the R0017M reagent system (Beyotime Biotechnology, Shanghai, China). Reverse transcription was performed utilizing the R323 kit (Vazyme, Nanjing, China) per the manufacturer's directions. Primer sequences are listed in Supplementary Table 1.

Western blot and co-immunoprecipitation: Proteins were isolated from both cells and tissues utilizing radio-immunoprecipitation assay lysis buffer (WB3100, New Cell and Molecular Biotech, Suzhou, China). Protein concentrations were measured *via* the bicinchoninic acid assay (WB6501, same supplier). The samples were resolved by sodium-dodecyl sulfate gel electrophoresis and subsequently transferred onto polyvinylidene fluoride membranes (IPFL00010, Merck Millipore, MA, United States). The membranes were blocked for 30 minutes at room temperature using rapid blocking buffer (P30500), followed by overnight incubation at 4 °C with primary antibodies. After three (10 minutes duration) washes with tris-buffered saline with Tween, the membranes were incubated with horseradish peroxidase-conjugated secondary antibodies (WB20500) at room temperature for 1 hour. Protein bands were detected using enhanced chemiluminescence substrate (P10300), and signal intensities were quantified employing ImageJ software (National Institutes of Health, MD, United States).

The following primary antibodies were used. Most were sourced from Proteintech, China: Cysteine-aspartic acid protease-3 (Caspase-3) (1:1000, 19677-1-AP), Bcl-2 associated X protein (Bax) (1:10000, 50599-2-Ig), tumor necrosis factor-α (TNF-α) (1:1000, 17590-1-AP), glyceraldehyde-3-phosphate dehydrogenase (1:10000, 10494-1-AP), interleukin-6 (IL-6) (1:1000, 21865-1-AP), epithelial-cadherin (E-cadherin) (1:20000, 20874-1-AP), transforming growth factor-β1 (TGF-β1) (1:10000, 81746-2-RR), α-smooth muscle actin (α-SMA) (1:10000, 14395-1-AP), GSH peroxidase 4 (GPX4) (1:1000, 30388-1-AP), immunoglobulin G (1:1000, 11541-1-AP), and ubiquitin (1:2000, 10201-2-AP). Additional antibodies were obtained from Affinity, Shanghai, China: Solute carrier family 7 member 11 (SLC7A11) (1:1000, DF12509), autophagy related 7 (ATG7) (1:1000, DF6130), sequestosome 1 (SQSTM1) (1:500, AF5384), and microtubule-associated protein 1A/1B-light chain 3 (LC3) (1:1000, AF5402). Moreover, homologous to E6-AP C-terminus and RCC1-like domain-containing E3 ubiquitin protein ligase (HERC2) antibody (1:500, CY-15460R) was sourced from Shanghai Caiyou Industry Co., Ltd., Shanghai, China; ferritin heavy chain 1 (FTH1) antibody (1:500, sc-376594) was acquired from Santa Cruz Biotechnology, CA, United States; and nuclear receptor coactivator 4 (NCOA4) antibodies were procured from Beijing Novus, Beijing, China (1:1000, ab314553, Abcam, MA, United States; 1:1000, H00008031-M04G).

HK-2 cells underwent lysis on ice for 30 minutes employing weak radio-immunoprecipitation assay lysis buffer (P0013D, Beyotime, Shanghai, China). The lysates subsequently were centrifuged for 20 minutes at 4 °C, and the supernatants were collected. These were then incubated for entire night at 4 °C with gentle shaking in the presence of the appropriate primary antibody. Co-immunoprecipitation (Co-IP) was performed according to the Protein A-Agarose kit protocol (P2051, Beyotime, Shanghai, China). Immunoprecipitates were resuspended in 1 × sodium-dodecyl sulfate gel electrophoresis loading buffer (P0015A, Beyotime, Shanghai, China), and protein expression was analyzed by Western blot per standard procedures.

Cell transfection: Plasmids for HERC2 overexpression, NCOA4 knockdown, and their respective negative controls were designed and produced by Sangon Biotech (Shanghai, China). HK-2 cells were transfected per the manufacturer's protocols (Sangon Biotech, Shanghai, China). Transfection efficiency exceeding 70% was confirmed by quantitative reverse transcription-polymerase chain reaction (qRT-PCR) and immunoblotting, and successfully transfected cells were used for subsequent experiments. After 24 hours of transfection, cells were treated with varying concentrations of KKBS.

Immunofluorescence: Cells were treated with 4% paraformaldehyde (P0099-3 L, Beyotime, Shanghai, China) for fixation and subsequently permeabilized with 0.1% Triton X-100 (ST795, Beyotime, Shanghai, China) for 30 minutes at room temperature. Antigen blocking was performed by incubating cells with fluorescence-blocking solution (P0260, Beyotime, Shanghai, China) for 30 minutes. Moreover, primary antibodies were employed overnight at 4 °C under a humidified environment. After washing, fluorescein isothiocyanate-conjugated (P0196, Beyotime, Shanghai, China) and Cy3-labeled (P0183, Beyotime, Shanghai, China) secondary antibodies were incubated for 1 hour in the dark at 25 °C. Nuclei were counterstained using DAPI (C1005, Beyotime, Shanghai, China) for 10 minutes protected from light, followed by three

washes with phosphate buffered saline. Additionally, fluorescent images were captured using a Nikon DS-Fi2 inverted epifluorescence microscope equipped with multiband filter sets.

Animal experimentation: The db/db mouse model, carrying a leptin receptor gene mutation causing obesity and type 2 diabetes mellitus, is widely used to study DKD. These mice develop obesity, hyperglycemia, hyperlipidemia, and glucosuria around 4 weeks, with DKD pathology emerging by about 8 weeks[31], closely mirroring human disease progression. Male db/db and wild-type db/m control mice (8 weeks old) were obtained from Jiangsu Ailingfei Biotechnology Co., Ltd, Jiangsu, China. All animals were housed under specific pathogen-free conditions at 22 ± 2 °C, 35% ± 5% humidity, and 12-hour light/dark cycles, with free access to standard feed and autoclaved water. For this research, all procedures were approved by the Institutional Animal Care Committee of Affiliated Hospital of Nanjing University of Chinese Medicine (No. 2023DW-039-02) and conducted per international animal welfare guidelines.

Animal grouping and model establishment: The db/m mice served as non-diabetic controls. The db/db mice were divided into four experimental groups (n = 8 per group): (1) Vehicle-treated model group (0.5% carboxymethylcellulose); (2) Low-dose KKBS (L-KKBS) intervention (11.05 g/kg body weight, oral gavage); (3) High-dose KKBS (H-KKBS) intervention (22.1 g/kg, oral gavage); and (4) Positive control group (irbesartan, 1.36 g/kg, daily gavage). After a 7-day acclimation period, fasting blood glucose levels were determined employing precision glucometry. Simultaneously, 24-hour urine samples were harvested in metabolic cages. DKD was confirmed by meeting both diagnostic criteria: Fasting blood glucose ≥ 16.7 mmol/L and urinary albumin-to-creatinine ratio (UACR) ≥ 30 mg/g, consistent with established guidelines[32].

Histopathological examination of renal tissue: Kidney tissues were paraffin-embedded, sectioned into 4 μm slices, and deparaffinized with xylene. After rehydration, sections were subjected to various histological stains: (1) Hematoxylin and eosin (HE) for cellular structure; (2) Periodic acid-Schiff (PAS) for glycogen detection; (3) Oil Red O for lipid droplet visualization; (4) Terminal deoxynucleotidyl transferase-mediated deoxyuridine triphosphate-nick end labelling assay to assess apoptosis; and (5) Masson's trichrome for collagen deposition. All staining procedures followed manufacturer instructions. Sections were scrutinized under the bright-field microscope (Nikon Eclipse Ci-L, Tokyo, Japan), and representative images were captured using NIS-Elements imaging software. Additionally, 1 mm^3 kidney samples from each group were collected for ultrastructural analysis of mitochondrial morphology *via* transmission electron microscopy (TEM).

Immunohistochemical staining: Paraffin-embedded tissue sections, processed as for histological staining, underwent antigen retrieval in citrate buffer (pH = 6.0). Endogenous peroxidase activity was inhibited using 3% H_2O_2, then nonspecific binding sites were blocked with 5% bovine serum albumin at 37 °C for 1 hour. Tissue sections were immersed overnight at 4 °C in a solution of primary antibodies diluted in the suitable buffer. After three washes with tris-buffered saline with Tween, horseradish peroxidase-conjugated secondary antibodies were employed for 30 minutes at room temperature. Chromogenic detection was conducted utilizing diaminobenzidine substrate (DAB0031, Maixin Bio, Fuzhou, China), with reaction time optimized under microscopic observation. Nuclei were counterstained with Mayer's hematoxylin (G1080, Servicebio, Wuhan, China) for 30 seconds before dehydration through graded ethanol and clearing in xylene. Whole-slide images were acquired with an Olympus VS200 slide scanner using a 40 × objective (0.75 NA) under standardized settings.

Statistical analysis

Results are shown as the mean ± SD. Statistical analyses were conducted using GraphPad Prism 9.0 (GraphPad Software, San Diego, CA, United States). For comparisons of multiple groups, one-way ANOVA was utilized, followed by Tukey's *post hoc* test. Before analysis, data were checked for normality utilizing the Shapiro-Wilk test and for equal variances by the Levene's test. When these assumptions were not met, non-parametric methods, Kruskal-Wallis test with Dunn's multiple comparisons, were used. A P value < 0.05 was deemed statistically significant. Missing data were not subjected to imputation. Samples with missing values due to experimental errors were excluded on a case-by-case basis; final sample sizes (n) are reported in figure legends and results. All experiments were independently conducted a minimum of three times to guarantee reproducibility.

RESULTS

KKBS improves renal function and mitigates renal tissue damage in db/db mice

To evaluate the renal protective efficacy of KKBS, we used db/db mice as a model of DKD. After 12 weeks of KKBS treatment (Figure 1A), db/db mice had higher body weight, blood glucose levels, and UACR compared to db/m mice (P < 0.05). Both irbesartan and KKBS significantly reduced body weight and UACR in db/db mice, whereas blood glucose levels showed a minimal change (Figure 1B-D). Regarding renal function, the db/db mice displayed a significantly elevated kidney index compared to db/m controls (P < 0.01). KKBS treatment notably decreased the kidney index (P < 0.05), while irbesartan did not cause a statistically significant change (Figure 1E). Similar levels of hepatic transaminases (alanine aminotransferase and aspartate aminotransferase) across all groups indicated the *in vivo* safety of KKBS treatment (Figure 1F and G). L-KKBS significantly reduced serum creatinine levels (P < 0.05), whereas H-KKBS had no significant effect (Figure 1H). However, both H-KKBS and L-KKBS markedly decreased 24-hour urine total protein and

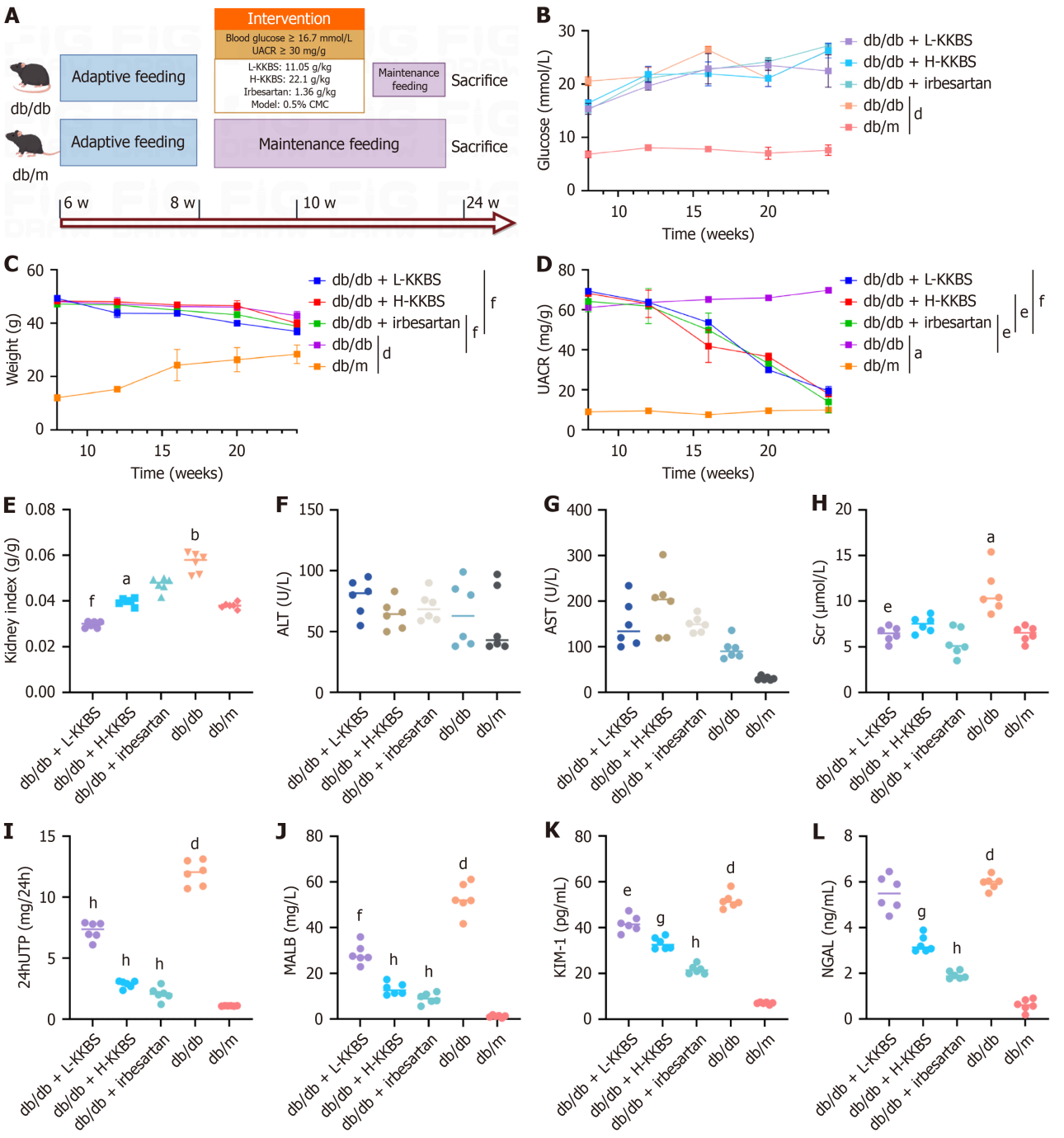


Figure 1 Kunkui Baoshen decoction improves renal function in db/db mice. A: Experimental design and timeline showing db/db mouse model establishment and drug intervention schedule; B-D: Longitudinal monitoring of fasting blood glucose levels, body weight, and urinary albumin-to-creatinine ratio at 4-week intervals during the 12-week treatment period; E: Biochemical assessment after 12 weeks of treatment: Kidney index (kidney weight/body weight ratio); F and G: Liver function markers: Alanine aminotransferase and aspartate aminotransferase; H: Serum creatinine; I: 24-hour urinary total protein; J: Urinary malondialdehyde; K: Kidney injury molecule-1; L: Neutrophil gelatinase-associated lipocalin. UACR: Urinary albumin-to-creatinine ratio; L-KKBS: Low-dose Kunkui Baoshen decoction; H-KKBS: High-dose Kunkui Baoshen decoction; CMC: Carboxymethylcellulose; ALT: Alanine aminotransferase; AST: Aspartate aminotransferase; Scr: Serum creatinine; 24hUTP: 24-hour urinary total protein; MALB: Malondialdehyde; KIM-1: Kidney injury molecule-1; NGAL: Neutrophil gelatinase-associated lipocalin. $^{a}P < 0.05$ *vs* db/m group, $^{b}P < 0.01$ *vs* db/m group, $^{d}P < 0.0001$ *vs* db/m group; $^{e}P < 0.05$ *vs* db/db group, $^{f}P < 0.01$ *vs* db/db group, $^{g}P < 0.001$ *vs* db/db group, and $^{h}P < 0.0001$ *vs* db/db group.

urinary malondialdehyde levels ($P < 0.01$; Figure 1I and J), suggesting improved renal function in treated db/db mice.

Neutrophil gelatinase-associated lipocalin and kidney injury molecule-1 are established biomarkers of tubular damage [33]. Both markers were markedly increased in the db/db group relative to db/m controls ($P < 0.0001$). Treatment with KKBS significantly reduced their expression, with a pronounced decrease in kidney injury molecule-1 observed in the L-KKBS group ($P < 0.05$), while neutrophil gelatinase-associated lipocalin reduction was less marked (Figure 1K and L). These findings support the conclusion that KKBS ameliorates renal function in db/db mice.

Table 1 Name and weight of Chinese herbs in Kunkui Baoshen decoction

No.	Chinese name	Scientific name	Weight
1	Huangqi	*Astmgali Radix*	30 g
2	Huobahuagen	*Tripterygium hypoglaucum*	15 g
3	Jiuyurou	*Fructus Ligustri Lucidi*	10 g
4	Huangshukuihua	*Corni Fructus Preparata*	30 g

Further, histopathological examinations were performed to assess KKBS's protective effects on renal tissue. HE staining demonstrated notable pathological alterations in db/db mice compared to db/m controls, including mesangial matrix thickening and expansion, tubular edema with vacuolization, and prominent interstitial inflammatory cell infiltration. In contrast, the KKBS and irbesartan-treated groups showed no evident mesangial proliferation, only mild tubular edema, and reduced inflammatory infiltration ($P < 0.01$; Figure 2A). PAS staining corroborated these observations: Db/db mice displayed enlarged mesangial cells, matrix proliferation, disrupted tubular architecture, and interstitial inflammation ($P < 0.01$), all of which were significantly alleviated by KKBS treatment as evidenced by a decreased mesangial matrix area ($P < 0.01$; Figure 2B). Masson's trichrome staining indicated enhanced collagen accumulation in the tubular basement membrane and interstitium of db/db mice compared to controls ($P < 0.001$), while the H-KKBS and irbesartan groups showed significantly reduced collagen accumulation ($P < 0.05$) (Figure 2C). In addition, Oil Red O staining demonstrated a higher number of lipid droplets in db/db mice relative to db/m mice ($P < 0.01$). Both KKBS and irbesartan treatments effectively attenuated lipid droplet deposition ($P < 0.01$; Figure 2D). Collectively, these findings suggest that KKBS improves renal function and mitigates renal tissue damage in db/db mice.

KKBS alleviates inflammation, fibrosis, and cellular apoptosis in vitro and in vivo

To further validate the anti-fibrotic effects of KKBS in DKD, inflammatory and fibrotic markers (TGF-β1, IL-6, TNF-α, E-cadherin, and α-SMA) were assessed both *in vivo* and *in vitro*. *In vivo*, the db/db group had significantly elevated expression of TGF-β1 ($P < 0.01$), IL-6 ($P < 0.01$), TNF-α ($P < 0.0001$), and α-SMA ($P < 0.001$), accompanied by decreased E-cadherin levels ($P < 0.001$) compared to the db/m group. KKBS treatment markedly reduced the expression of these fibrotic and inflammatory markers ($P < 0.01$). Terminal deoxynucleotidyl transferase-mediated deoxyuridine triphosphate-nick end labelling staining revealed significantly raised apoptosis in the renal tissue of db/db mice ($P < 0.0001$), which was substantially attenuated by both KKBS and irbesartan treatments ($P < 0.05$; Figure 3). These results suggest that KKBS mitigates renal fibrosis by modulating inflammation, fibrosis, and apoptosis.

In vitro, the renal protective effects of KKBS were evaluated in HK-2 cells using a CCK-8 assay under varying glucose conditions. Cell viability was significantly reduced at 50 mmol/L glucose ($P < 0.0001$; Figure 4A), which was therefore selected for subsequent experiments. A 50 mmol/L mannitol group was included to control for potential osmotic effects. KKBS treatment significantly improved cell viability under HG conditions, with the greatest effect observed at 0.1 g/mL ($P < 0.0001$) compared to the HG group (Figure 4B). Morphological analysis showed that cells in the normal glucose (5.5 mmol/L) group maintained the typical cobblestone-like morphology, whereas cells exposed to HG (50 mmol/L glucose) exhibited irregular, spindle-shaped morphology with increased intercellular spacing. KKBS treatment (50 mmol/L glucose + 14% KKBS) largely restored the cobblestone-like morphology and reduced cell spacing (Figure 4C). Scratch assays demonstrated that HG induced HK-2 cell migration ($P < 0.001$), which was significantly inhibited by KKBS treatment ($P < 0.001$; Figure 4D and E).

Western blot and qRT-PCR analyses revealed significant upregulation of the apoptotic markers Caspase-3 and Bax under HG conditions ($P < 0.0001$). KKBS treatment significantly decreased Caspase-3 and Bax protein levels ($P < 0.01$; Figure 4F-I), although Bax mRNA expression was not significantly altered. These results suggest that KKBS reduces HG-induced apoptosis by downregulating key apoptotic proteins. Furthermore, pro-inflammatory cytokines (TNF-α and IL-6) were raised in the HG group ($P < 0.01$) but significantly decreased following KKBS treatment ($P < 0.05$; Figure 4J-L), with qRT-PCR data confirming similar trends ($P < 0.001$; Figure 4M). Fibrosis-related markers were also affected by HG, with decreased E-cadherin ($P < 0.01$) and increased α-SMA and TGF-β1 expression ($P < 0.01$). KKBS treatment reversed these changes, restoring marker levels toward normal ($P < 0.01$; Figure 4N-Q), supported by corresponding qRT-PCR results (Figure 4R). Collectively, these results demonstrate that KKBS exerts renoprotective effects in HG-induced HK-2 cells by inhibiting apoptosis, inflammation, migration, and fibrosis-associated marker expression.

Metabonomics analysis of mechanism of action of KKBS in DKD

To investigate the mechanism of KKBS against DKD, metabolomics analysis was performed. LC-MS/MS was employed in full scan mode to generate a compound fingerprint of KKBS (Supplementary Figure 1A and B). Following systematic data matching and manual validation, nine compounds were identified: Secologanin, sweroside, calycosin 7-O-β-D-glucoside, isoquercetin, quercetin, myricetin, kaempferol, ononin, and formononetin (Figure 5A and B). These compounds are listed in detail in Table 2. The experimental procedures and quantification of these compounds in KKBS are provided in Supplementary Table 2.

Metabolomics analysis revealed that the sample correlation heatmap (Figure 5C) showed a strong resemblance in both metabolic composition and abundance among the three KKBS plasma samples from db/db mice (KKBS1, KKBS2, and KKBS3). Principal component analysis further demonstrated clear separation between the KKBS and control groups, with

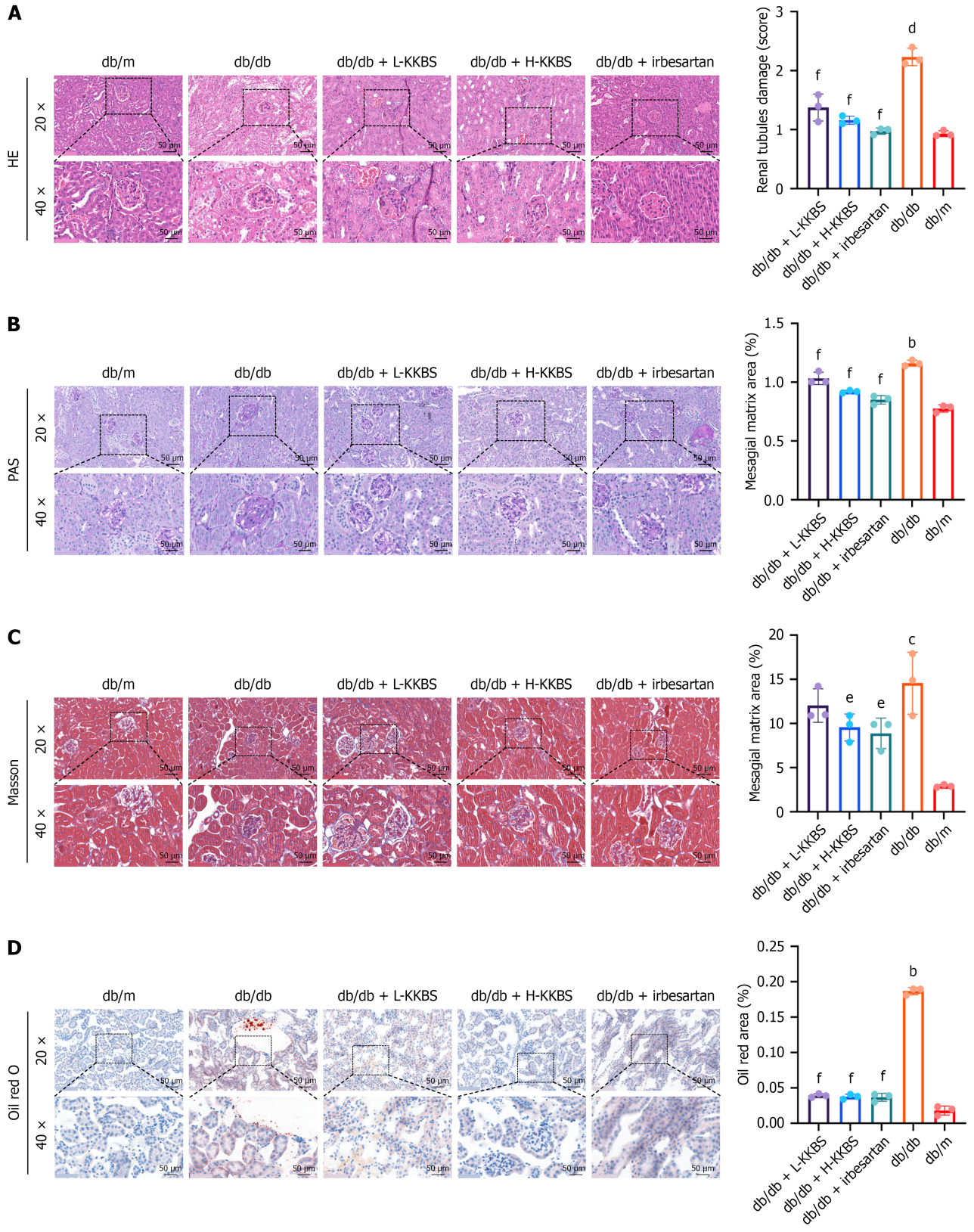


Figure 2 Kunkui Baoshen decoction alleviates renal tissue damage in db/db mice. Histopathological evaluation of renal tissues using various staining techniques at magnifications of 20 × and 40 × (scale bars = 50 μm) and quantitative analyses across all groups. A: Hematoxylin and eosin staining to assess overall tissue architecture and renal tubular damage; B: Periodic acid-Schiff staining to evaluate glomerular basement membrane thickening and mesangial expansion; C: Masson's trichrome staining to identify collagen deposition and renal fibrosis; D: Oil Red O staining to visualize lipid accumulation in kidney tissues. L-KKBS: Low-dose Kunkui Baoshen decoction; H-KKBS: High-dose Kunkui Baoshen decoction; HE: Hematoxylin and eosin; PAS: Periodic acid-Schiff. $^{b}P < 0.01$ *vs* db/m group, $^{c}P < 0.001$ *vs* db/m group, $^{d}P < 0.0001$ *vs* db/m group; $^{e}P < 0.05$ *vs* db/db group, and $^{f}P < 0.01$ *vs* db/db group.

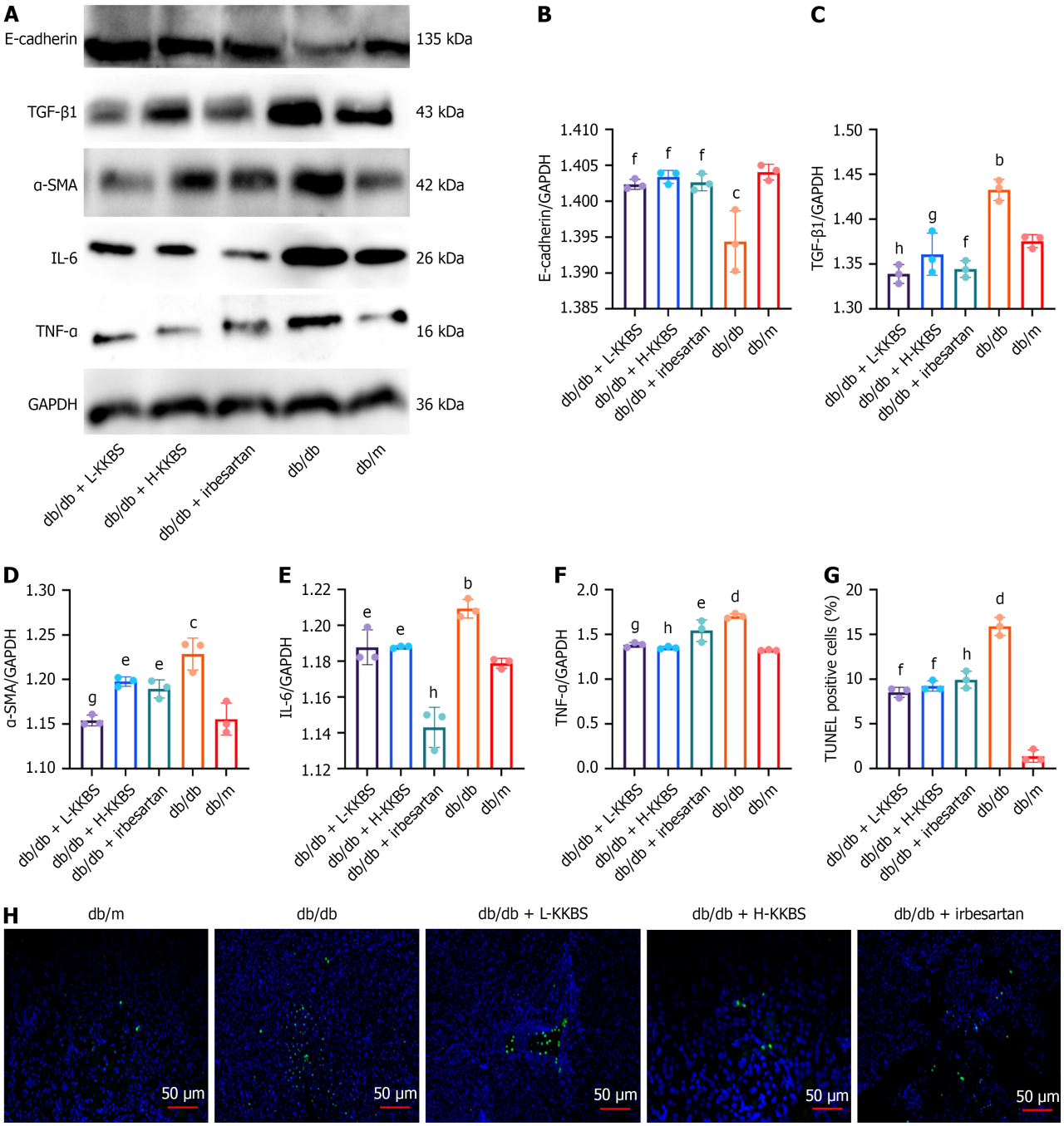
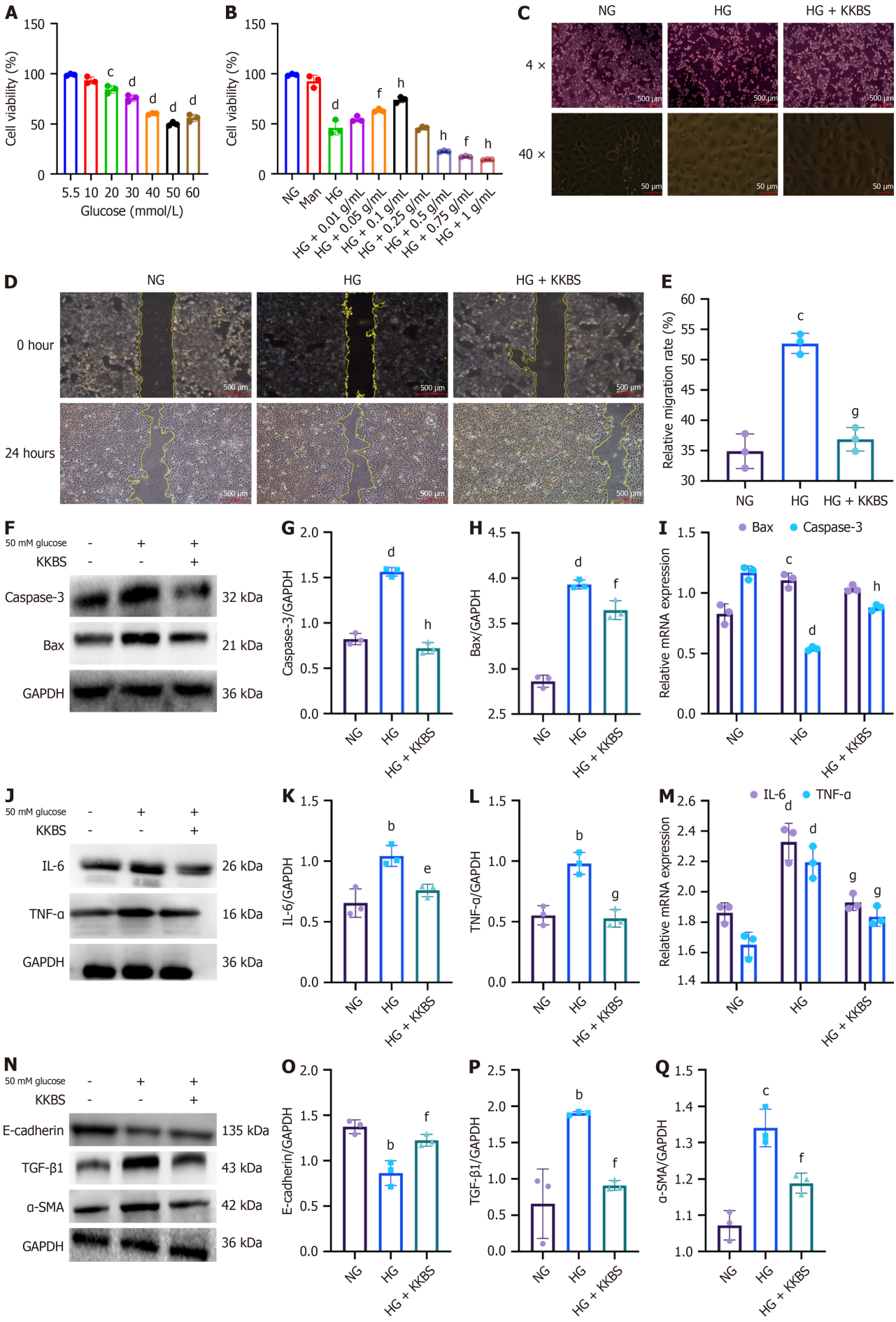


Figure 3 Kunkui Baoshen decoction alleviates inflammation, fibrosis, and cellular apoptosis in renal tissue of db/db mice. A-G: Quantification of key inflammatory and fibrotic markers in renal tissues across five groups, including: Transforming growth factor-β1, interleukin-6, tumor necrosis factor-α, epithelial-cadherin, and α-smooth muscle actin; H: Assessment of renal tubular epithelial cell apoptosis using terminal deoxynucleotidyl transferase-mediated deoxyuridine triphosphate-nick end labelling staining. Representative images are shown for each group (scale bars = 50 μm). E-cadherin: Epithelial-cadherin; TGF-β1: Transforming growth factor-β1; α-SMA: α-smooth muscle actin; IL-6: Interleukin-6; TNF-α: Tumor necrosis factor-α; GAPDH: Glyceraldehyde 3-phosphate dehydrogenase; L-KKBS: Low-dose Kunkui Baoshen decoction; H-KKBS: High-dose Kunkui Baoshen decoction; TUNEL: Terminal deoxynucleotidyl transferase-mediated deoxyuridine triphosphate-nick end labelling. $^{b}P < 0.01$ *vs* db/m group, $^{c}P < 0.001$ *vs* db/m group, $^{d}P < 0.0001$ *vs* db/m group; $^{e}P < 0.05$ *vs* db/db group, $^{f}P < 0.01$ *vs* db/db group, $^{g}P < 0.001$ *vs* db/db group, and $^{h}P < 0.0001$ *vs* db/db group.

principal component 1, which accounts for 72.40% of the variance and principal component 2, which accounts for 15.0% (Figure 5D). Increased intergroup distances corresponded to greater metabolic differences. Additionally, partial least squares discriminant analysis highlighted a significant classification distinction between the KKBS and control groups (Figure 5E). The partial least squares discriminant analysis permutation test used R^2Y and Q^2 values to evaluate the model's explanatory and predictive power, respectively, where higher cumulative R^2Y and Q^2 values indicate better model stability and reliability. Notably, an R^2Y value of 0.05 suggested that the explanatory power of the random model exceeded that of the original model during permutation testing (Figure 5F). Pathway analysis revealed that KKBS mainly affected GSH metabolism, lipid metabolism, and amino acid metabolism and the production of secondary metabolites (Figure 5G). Importantly, GSH metabolism is known to be a key pathway altered during ferroptosis[34].


A
Cell viability (%)
Glucose (mmol/L)
5.5 10 20 30 40 50 60
B
Cell viability (%)
NG
Man
HG
HG + 0.01 g/mL
HG + 0.05 g/mL
HG + 0.1 g/mL
HG + 0.25 g/mL
HG + 0.5 g/mL
HG + 0.75 g/mL
HG + 1 g/mL
C
NG
HG
HG + KKBS
4 ×
40 ×
D
0 hour
24 hours
E
Relative migration rate (%)
F
50 mM glucose
KKBS
Caspase-3
Bax
GAPDH
32 kDa
21 kDa
36 kDa
G
Caspase-3/GAPDH
H
Bax/GAPDH
I
Bax
Caspase-3
Relative mRNA expression
J
IL-6
TNF-α
26 kDa
16 kDa
K
IL-6/GAPDH
L
TNF-α/GAPDH
M
IL-6
TNF-α
N
E-cadherin
TGF-β1
α-SMA
135 kDa
43 kDa
42 kDa
O
E-cadherin/GAPDH
P
TGF-β1/GAPDH
Q
α-SMA/GAPDH

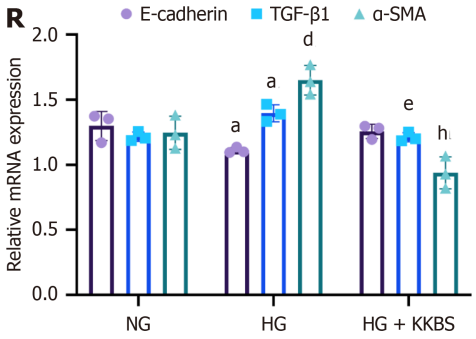


Figure 4 Kunkui Baoshen decoction alleviates inflammation, fibrosis, and cellular apoptosis in high glucose-induced human kidney-2 cells. A: Human kidney-2 (HK-2) cell viability under different glucose concentrations compared to the normal group (NG, 5.5 mmol/L glucose); B: HK-2 cell viability under high glucose (HG, 50 mmol/L glucose) with varying concentrations of Kunkui Baoshen decoction; C: Morphological changes of HK-2 cells observed at 4 × and 40 × magnification (scale bar = 500 μm); D: Wound healing assay to evaluate HK-2 cell migration under different treatments (scale bar = 500 μm); E: Quantification of migration rate; F-I: Western blot and quantitative reverse transcription-polymerase chain reaction (qRT-PCR) analyses of cysteine-aspartic acid protease-3 and Bcl-2 associated X protein in HK-2 cells; J-M: Western blot and qRT-PCR analyses of interleukin-6 and tumor necrosis factor-α in HK-2 cells; N-R: Western blot and qRT-PCR analyses of epithelial-cadherin, α-smooth muscle actin, and transforming growth factor-β1 in HK-2 cells. NG: Normal group; Man: Mannitol (osmotic control); HG: High glucose; KKBS: Kunkui Baoshen decoction; Caspase-3: Cysteine-aspartic acid protease-3; Bax: Bcl-2 associated X; GAPDH: Glyceraldehyde 3-phosphate dehydrogenase; IL-6: Interleukin-6; TNF-α: Tumor necrosis factor-α; E-cadherin: Epithelial-cadherin; TGF-β1: Transforming growth factor-β1; α-SMA: α-smooth muscle actin. $^{a}P < 0.05$ *vs* normal group, $^{b}P < 0.01$ *vs* normal group, $^{c}P < 0.001$ *vs* normal group, $^{d}P < 0.0001$ *vs* normal group; $^{e}P < 0.05$ *vs* high glucose group, $^{f}P < 0.01$ *vs* high glucose group, $^{g}P < 0.001$ *vs* high glucose group, $^{h}P < 0.0001$ *vs* high glucose group.

Transcriptomic analysis reveals the mechanism by which KKBS impacts DKD

Transcriptomic analysis provided deeper insight into the mechanisms by which KKBS affects DKD. The results of transcriptomic sequencing of renal tissue from KKBS-treated and db/db mice are summarized in Figure 6A. The volcano plot comparing the two groups identified 2354 upregulated and 984 downregulated genes (Figure 6B). Protein-protein interaction (PPI) network and KEGG pathway analyses revealed key DEGs including NCOA4, Janus kinase 2, CD44, CD40, and TNF, with NCOA4 emerging as the most significant hub in the PPI network (Figure 6C). These DEGs were significantly enriched in pathways such as ferroptosis, nuclear factor-κB signaling, and forkhead box O signaling (Figure 6D).

While the transcriptomic data substantially contributed to identifying potential targets and pathways modulated by KKBS, several limitations should be noted. The small sample size used for RNA sequencing may reduce the robustness and reproducibility of differential expression results, potentially hindering detection of subtle gene expression changes and increasing the risk of false positives and negatives. Additionally, confounding factors such as biological variability, batch effects, or minor differences in sample handling may have influenced gene expression profiles. Although standard procedures were employed to minimize these sources of variability, they remain inherent limitations of transcriptomic studies. Future research should include larger sample cohorts, technical replicates, and validation of key findings by quantitative PCR or protein-level assays to reinforce these conclusions.

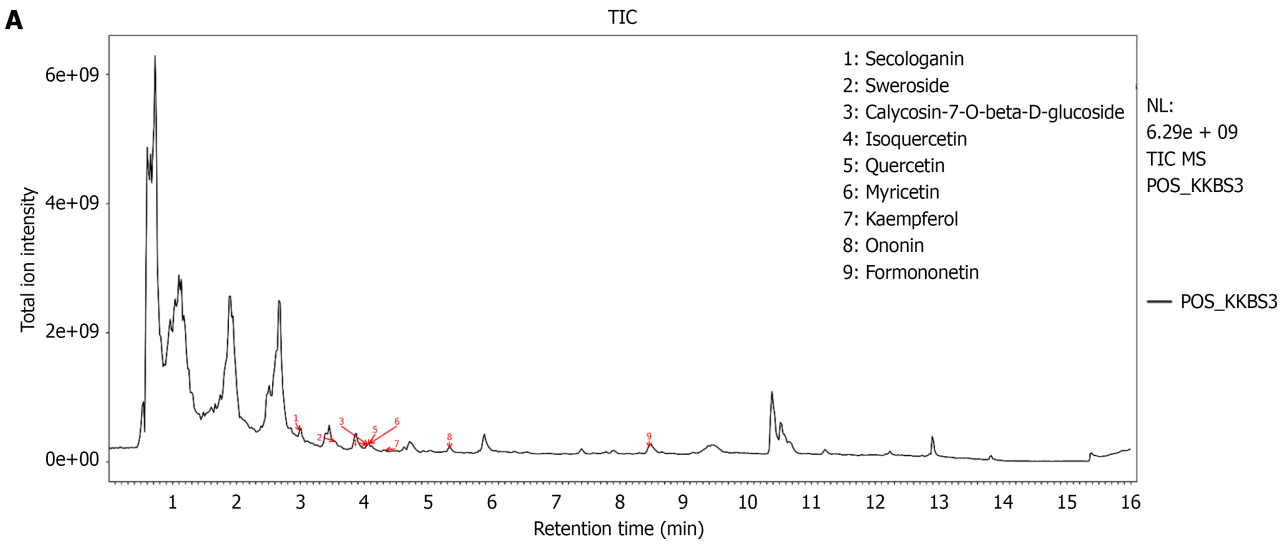
Metabonomics analysis and transcriptomics implicate ferroptosis pathway in DKD

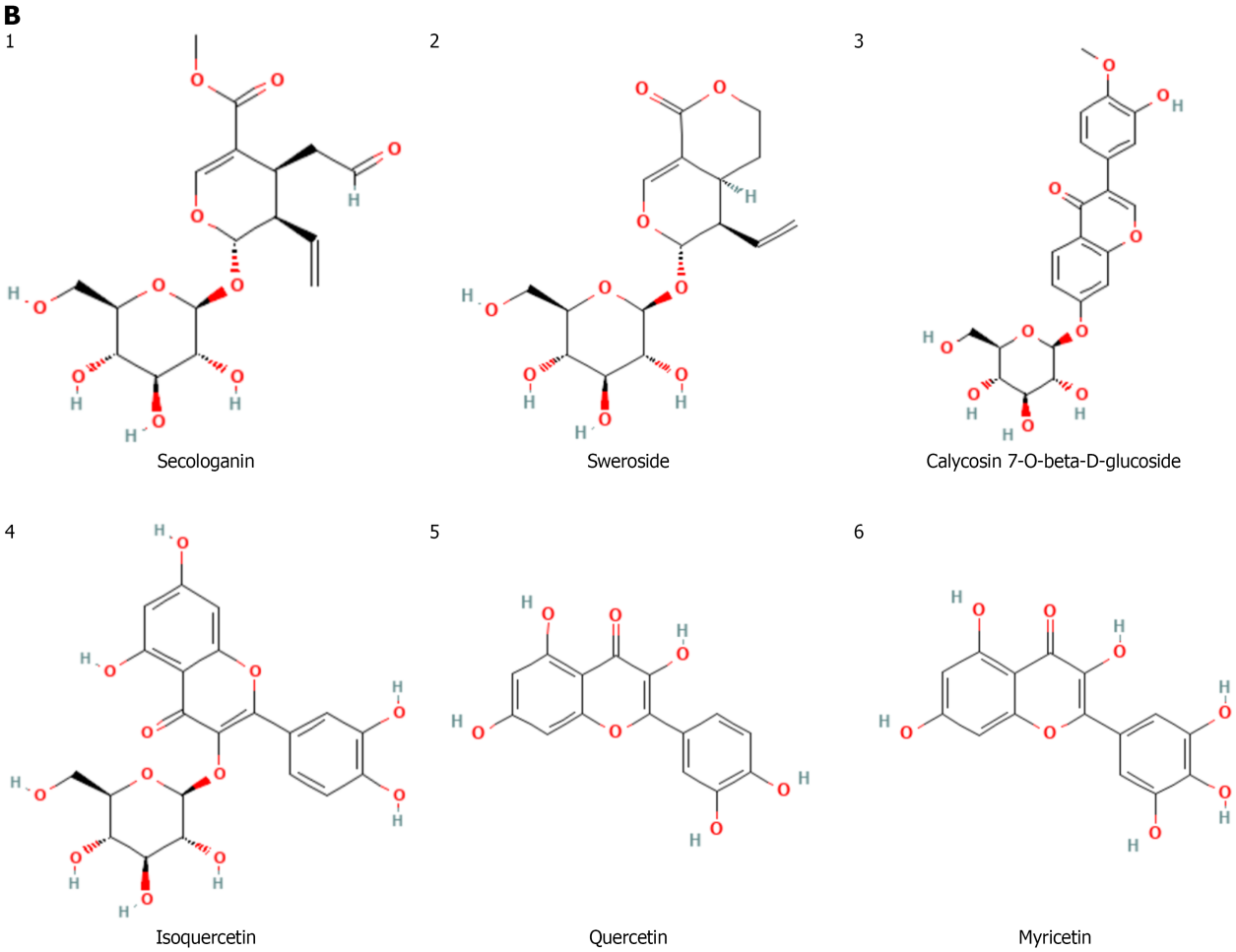
Comprehensive metabolomics analysis identified the GSH metabolic pathway as the most significant metabolic pathway associated with KKBS, which is also a key metabolic feature of ferroptosis. Integrating these results with transcriptomic data, we hypothesized that KKBS exerts its protective effects against DKD by inhibiting ferroptosis. Our experiments confirmed that, under HG conditions, HK-2 cells exhibited a significant rise in ROS ($P < 0.05$), iron ions (Fe^{2+}/Fe^{3+}; $P < 0.001$), and MDA ($P < 0.05$), accompanied by a marked decrease in the GSH/GSSG ratio ($P < 0.001$; Figure 7A-E). Both mRNA and protein expression levels of the ferroptosis markers GPX4 and SLC7A11 were significantly downregulated ($P < 0.05$), with GPX4 and SLC7A11 transcripts showing a particularly pronounced reduction ($P < 0.01$; Figure 7F-I). Collectively, these results suggest that ferroptosis is very substantial in fibrosis development in HG-induced HK-2 cells.

KKBS alleviates fibrosis by inhibiting ferroptosis in vitro and in vivo

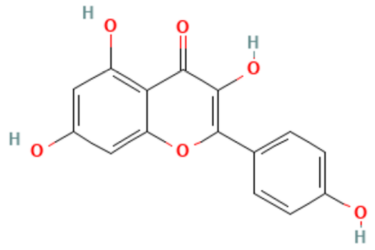
To investigate the effect of KKBS on the ferroptosis pathway, we measured ferroptosis biomarkers in renal tissues. Iron ions (Fe^{2+}/Fe^{3+}) were significantly elevated in the db/db group compared to the db/m group ($P < 0.0001$), accompanied by elevated levels of MDA ($P < 0.01$) and ROS, along with a marked reduction in the GSH/GSSG ratio ($P < 0.0001$). Treatment with KKBS and irbesartan significantly reduced Fe^{2+}/Fe^{3+} ($P < 0.05$), MDA ($P < 0.05$), and ROS levels, while increasing the GSH/GSSG ratio ($P < 0.05$; Figure 8A-D). TEM analysis further demonstrated that KKBS treatment significantly ameliorated ferroptosis-associated mitochondrial morphological changes, including organelle shrinkage, cristae loss, fragmentation, and increased membrane density (Figure 8E)[35].

In vitro experiments showed that combining KKBS with the ferroptosis inhibitor Fer-1 (10 μmol/L), used as a positive control, resulted in the HG + Fer-1 + KKBS group exhibiting significantly reduced ROS ($P < 0.05$), iron ions (Fe^{2+}/Fe^{3+}; $P < 0.001$), and MDA levels ($P < 0.001$) compared to the HG + Fer-1 group (Figure 9A-D). Additionally, the GSH/GSSG ratio was increased significantly ($P < 0.001$; Figure 9E). The expression of IL-6 (protein and mRNA) and TNF-α (protein) was also significantly decreased in the HG + Fer-1 + KKBS group ($P < 0.01$), although TNF-α mRNA levels remained un-


A
TIC
1: Secologanin
2: Sweroside
3: Calycosin-7-O-beta-D-glucoside
4: Isoquercetin
5: Quercetin
6: Myricetin
7: Kaempferol
8: Ononin
9: Formononetin
NL:
6.29e + 09
TIC MS
POS_KKBS3
POS_KKBS3
Total ion intensity
6e+09
4e+09
2e+09
0e+00
1 2 3 4 5 6 7 8 9 10 11 12 13 14 15 16
Retention time (min)

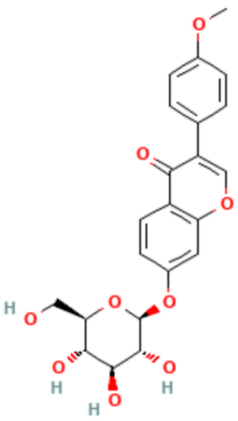

B
1
Secologanin
2
Sweroside
3
Calycosin 7-O-beta-D-glucoside
4
Isoquercetin
5
Quercetin
6
Myricetin

7



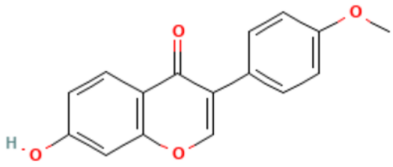
Kaempferol

8

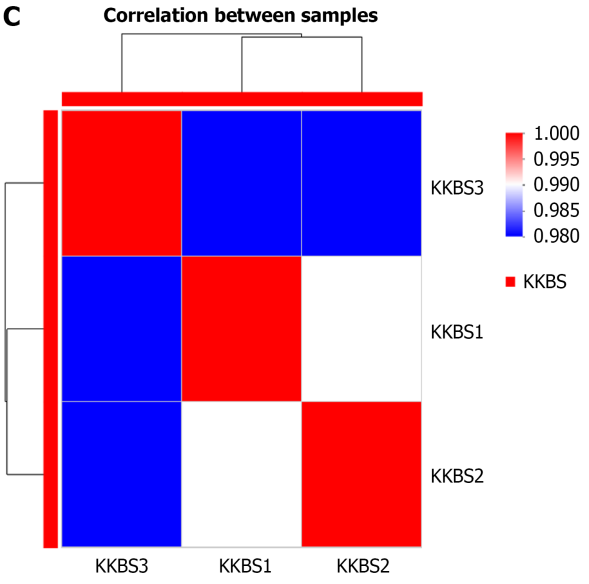


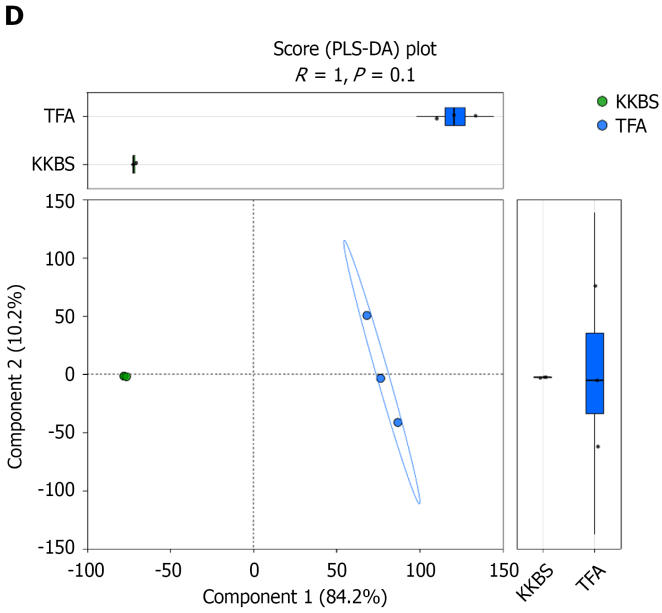
Ononin

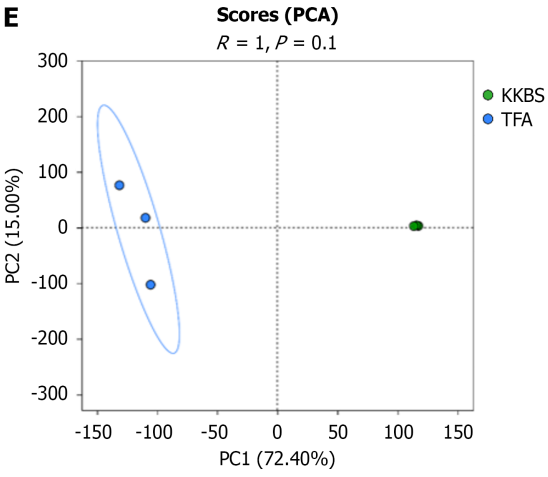
9

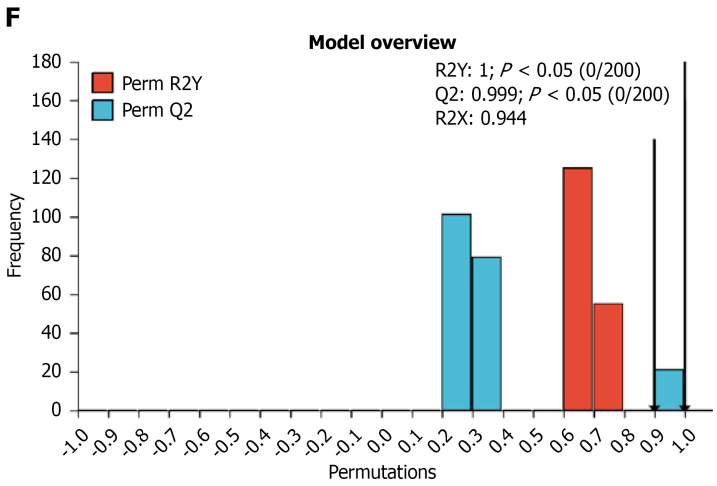


Formononetin









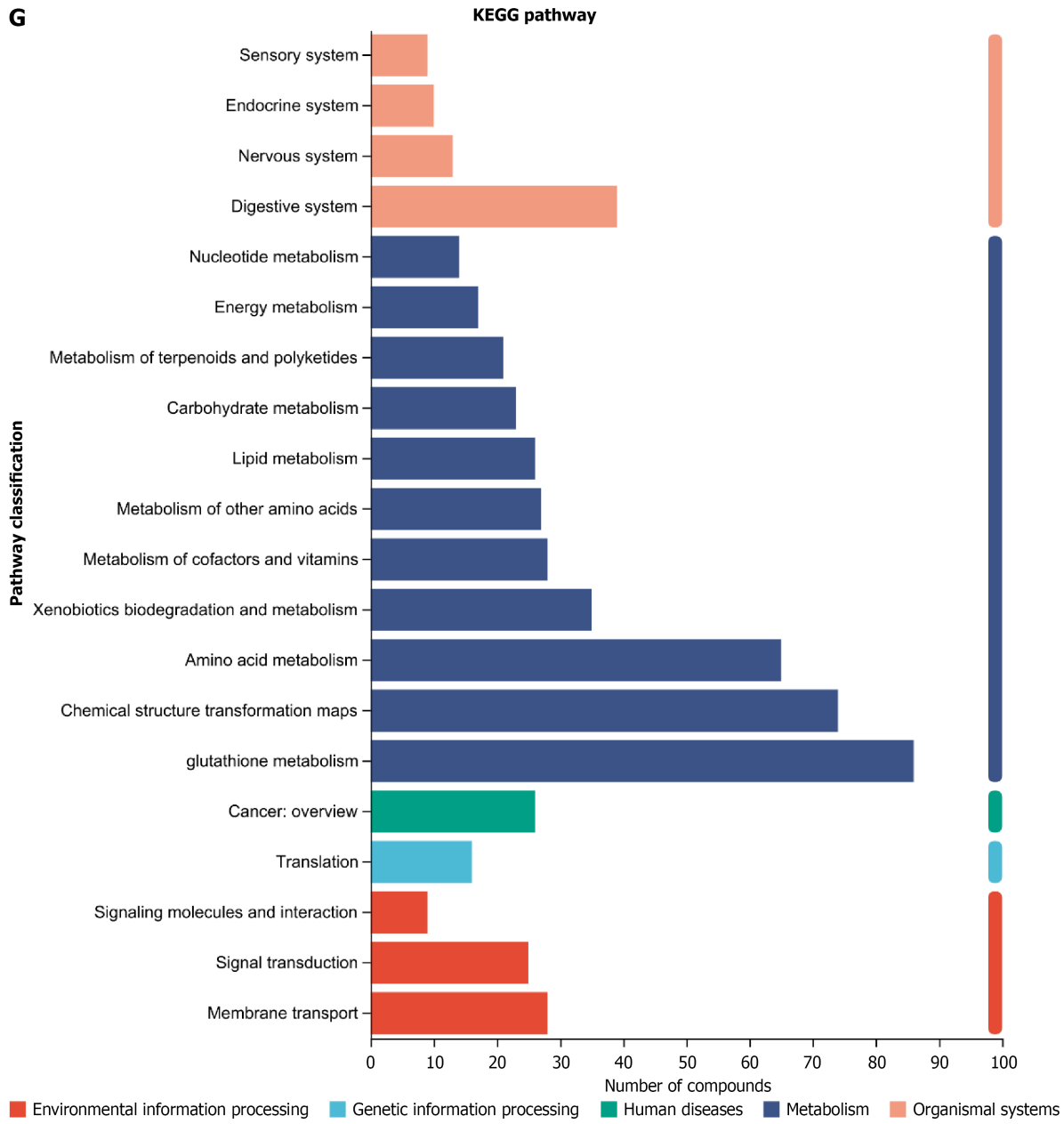


Figure 5 Component identification of Kunkui Baoshen decoction and metabolomics analysis. A: Total ion chromatogram of Kunkui Baoshen decoction (KKBS) obtained *via* liquid chromatography-mass spectrometry/mass spectrometry, showing the compound distribution profile; B: Representative chemical structures of key quality control components identified in KKBS; C: Sample correlation heatmap. Each cell represents the correlation coefficient between two samples. Color intensity indicates the strength of correlation, and hierarchical clustering (dendrograms on the top and side) reflects similarity—samples on the same branch are more similar to each other; D: Principal component analysis plot: Dimensionality reduction was performed to project samples onto principal components 1 and 2. The relative positions of points reflect similarity, and closer points indicate more similar metabolic profiles. Analysis of similarities was used to assess between-group differences. The *R* value (range: -1 to 1) indicates effect size, with values closer to 1 suggesting strong inter-group separation; the *P* value tests for significance; E: Partial least squares discriminant analysis score plot demonstrating group separation based on metabolite profiles. Component 1 and component 2 represent the major explanatory variables; F: Partial least squares discriminant analysis permutation test to evaluate the model's statistical reliability. The X-axis shows model accuracy, and the Y-axis shows the number of random permutations. Red bars = Q^2 values; blue bars = R^2Y values. *P* value = (number of permutations outperforming the original model)/(total permutations). A $P < 0.05$ indicates model validity; G: Kyoto Encyclopedia of Genes and Genomes (KEGG) pathway enrichment analysis. Bar graph showing the number of KKBS-related metabolites mapped to different KEGG pathways. The Y-axis shows KEGG subcategories, and the X-axis shows the number of mapped compounds. Pathways are grouped into seven categories: Metabolism, genetic information processing, environmental information processing, cellular processes, organismal systems, human diseases, and drug development, with distinct colors representing each category. TIC: Total ion chromatogram; PLS-DA: Partial least squares discriminant analysis; PCA: Principal component analysis; TFA: Total fatty acids; PC1: Component 1; PC2: Component 2; KKBS: Kunkui Baoshen decoction; KEGG: Kyoto Encyclopedia of Genes and Genomes.

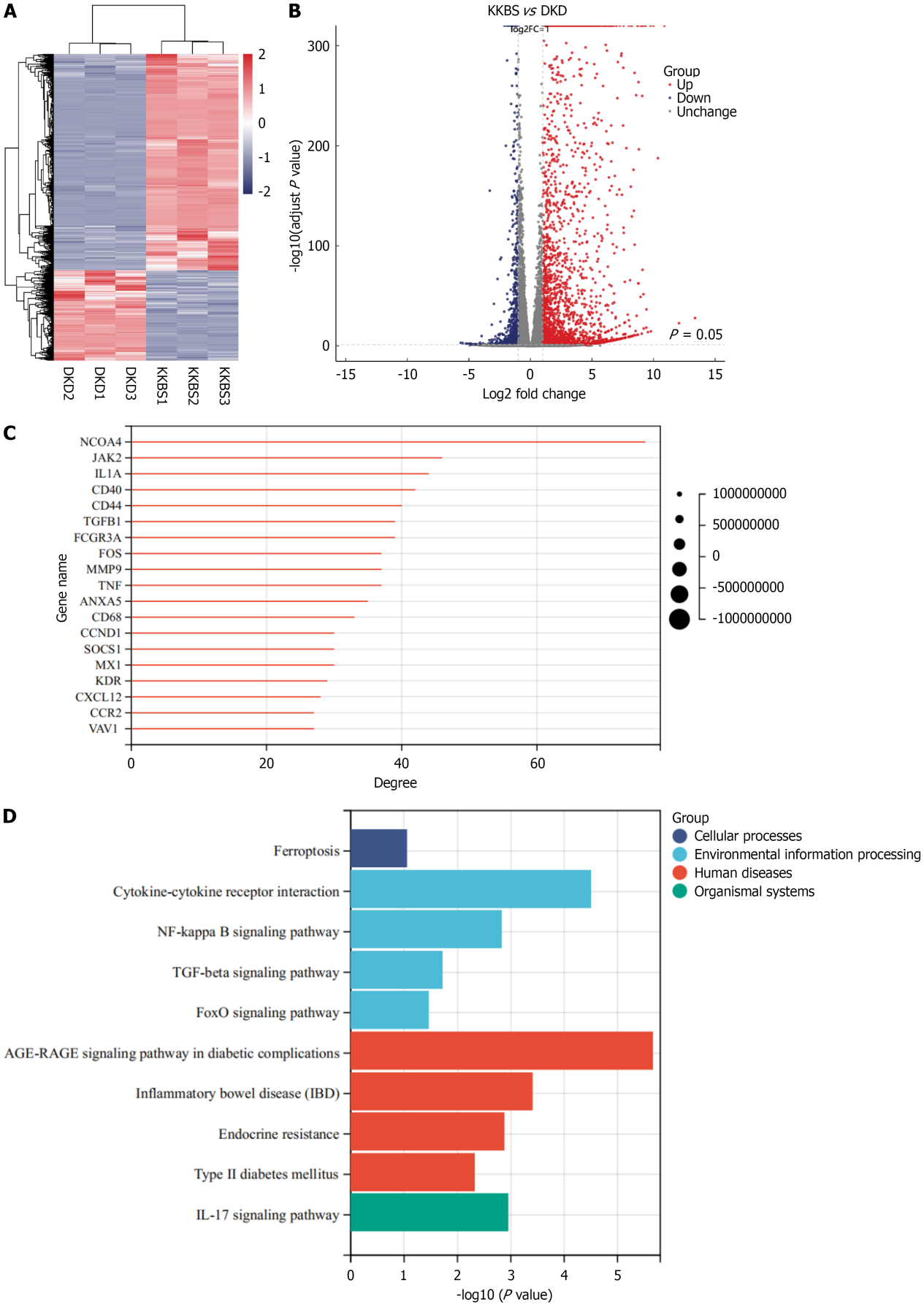


Figure 6 Transcriptomic analysis of renal tissues following Kunkui Baoshen decoction treatment. A: Hierarchical clustering heatmap of differentially expressed genes (DEGs) between the Kunkui Baoshen decoction treatment and db/db groups. Each column represents an individual sample, and each row

corresponds to a gene. Red indicates upregulation; blue indicates downregulation, visualizing distinct gene expression patterns between groups; B: Volcano plot of DEGs from transcriptomic sequencing comparing Kunkui Baoshen decoction and db/db groups. The X-axis represents the $\log_2$ fold change in gene expression, while the Y-axis indicates statistical significance ($-\log_{10}$ *P* value). Red points denote significantly upregulated genes, blue points indicate significantly downregulated genes, and gray points represent non-significant genes; C: The top 19 hub genes identified based on their degree values. The length of the red bars represents the degree score of each gene; the longer the bar, the more central the gene is within the network, suggesting a potentially greater regulatory role; D: Kyoto Encyclopedia of Genes and Genomes pathway enrichment analysis of the top DEGs from transcriptomic sequencing. The length of each bar reflects the relative importance of the pathway, with longer bars indicating more significant enrichment. KKBS: Kunkui Baoshen decoction; DKD: Diabetic kidney disease; NCOA4: Nuclear receptor coactivator 4; JAK2: Janus kinase 2; IL1A: Interleukin-1α; TGF-β1: Transforming growth factor-β1; FCGR3A: Fc gamma receptor IIIa; FOS: FBJ murine osteosarcoma viral oncogene homolog; MMP9: Matrix metalloproteinase 9; TNF: Tumor necrosis factor; ANXA5: Annexin A5; CCND1: Cyclin D1; SOCS1: Suppressor of cytokine signaling 1; MX1: Myxovirus resistance 1; KDR: Kinase insert domain receptor; CXCL12: C-X-C motif chemokine ligand 12; CCR2: C-C motif chemokine receptor 2; VAV1: Vav 1 oncogene; NF-κB: Nuclear facto-κB; FoxO: Forkhead box O; AGE-RAGE: Advanced glycation end products-receptor for advanced glycation end products; IL-17: Interleukin-17.

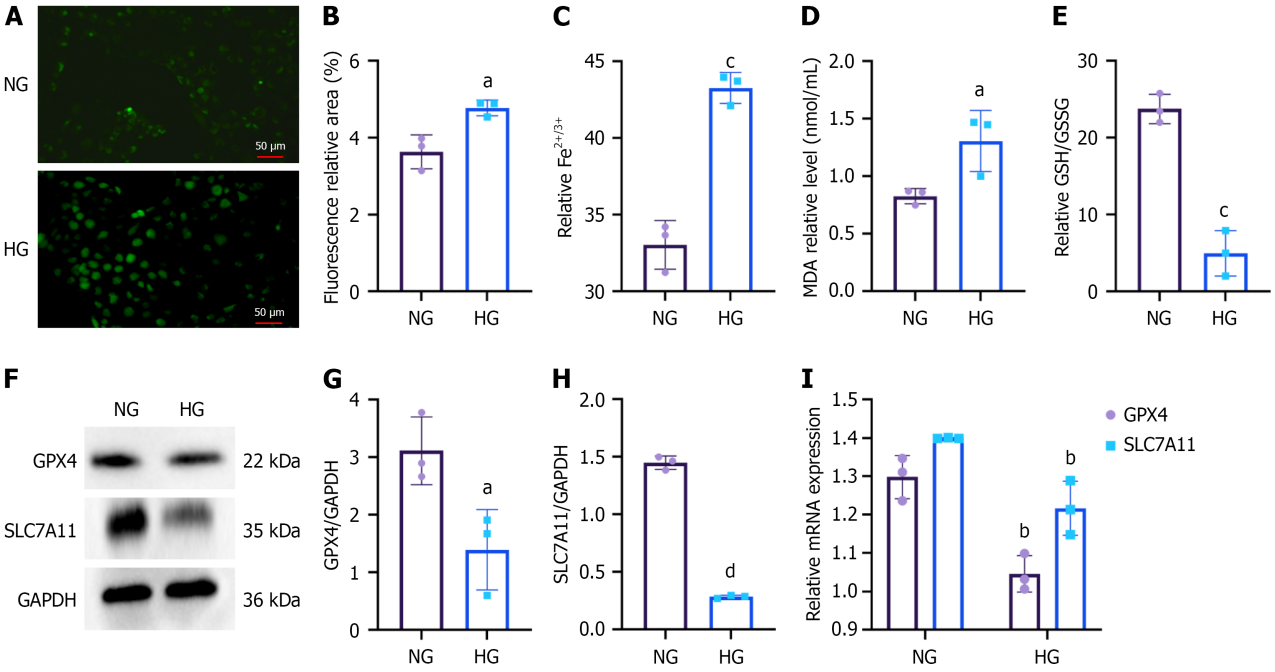


Figure 7 Ferroptosis in human kidney-2 cells under high-glucose conditions. A: Intracellular reactive oxygen species levels in the normal (NG) and high glucose (HG) groups were visualized using fluorescence microscopy (scale bars = 50 μm); B: Quantification of reactive oxygen species fluorescence intensity (expressed as relative fluorescent area%) in the NG and HG groups; C: Intracellular iron (Fe^{2+}/Fe^{3+}) levels in the NG and HG groups; D: Malondialdehyde levels in the NG and HG groups; E: Glutathione to oxidized glutathione ratio in the NG and HG groups; F-I: Expression levels of ferroptosis-related markers glutathione peroxidase 4 and recombinant solute carrier family 7 member 11 were analyzed by Western blot and quantitative reverse transcription-polymerase chain reaction in the NG and HG groups. NG: Normal group; HG: High glucose; MDA: Malondialdehyde; GSH: Glutathione; GSSG: Oxidized glutathione; GPX4: Glutathione peroxidase 4; SLC7A11: Solute carrier family 7 member 11; GAPDH: Glyceraldehyde 3-phosphate dehydrogenase. $^{a}P < 0.05$ *vs* normal group, $^{b}P < 0.01$ *vs* normal group, $^{c}P < 0.001$ *vs* normal group, and $^{d}P < 0.0001$ *vs* normal group.

changed (Figure 9F-I). Compared to the HG + Fer-1 group, the HG + KKBS group exhibited significantly improved expression of the fibrosis markers E-cadherin, α-SMA, and TGF-β1 at both the protein and mRNA levels ($P < 0.05$; Figure 9J-N). These findings indicate that KKBS alleviates fibrosis by inhibiting ferroptosis both *in vitro* and *in vivo*.

KKBS modulates ferroptosis by regulating NCOA4-mediated ferritinophagy

To elucidate how KKBS influences ferroptosis in HK-2 cells, we focused on *NCOA4*, identified by transcriptomic analysis as a key gene within the PPI network closely associated with the ferroptosis pathway. NCOA4, a selective autophagic cargo receptor, transports the NCOA4-ferritin complex to lysosomes, promoting ferritin degradation and releasing free iron, thereby inducing ferroptosis[36]. We assessed autophagic markers in HG-induced HK-2 cells and observed increased protein and mRNA levels of ATG7 in the HG group compared to the NG group ($P < 0.05$). NCOA4 and LC3 protein levels were elevated ($P < 0.05$), whereas SQSTM1/p62 and FTH1 Levels were decreased ($P < 0.05$). qRT-PCR results largely corroborated the Western blot findings, except for ATG7 and NCOA4 mRNA expression (Figure 10A-G). Immunofluorescence (IF) analysis revealed significant co-localization of NCOA4 and FTH1 under HG conditions, with an increased number of fluorescent foci (Figure 10H), indicating that ferritinophagy contributes to ferroptosis under these conditions.

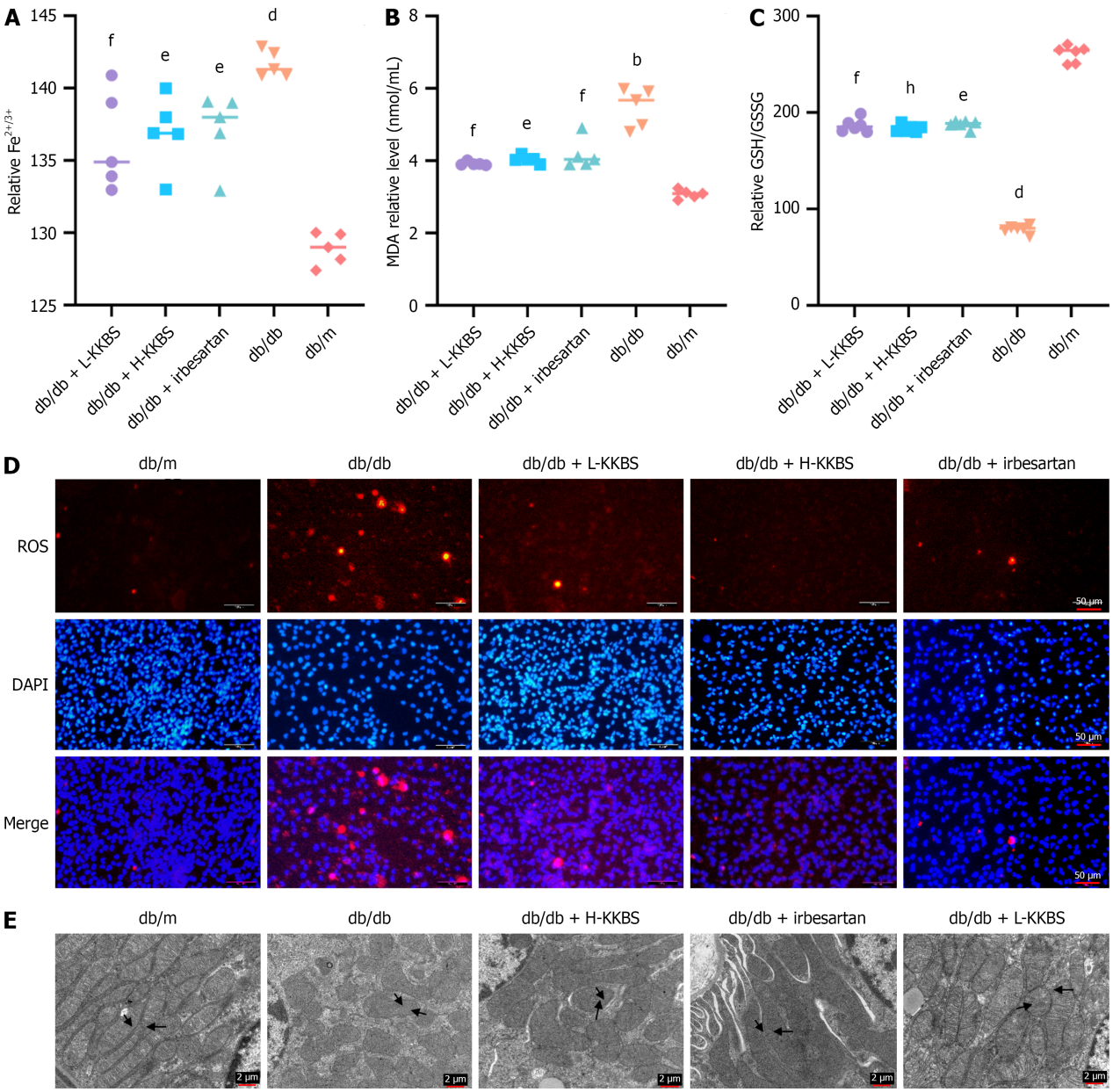


Figure 8 Kunkui Baoshen decoction alleviates fibrosis by inhibiting ferroptosis *in vitro* and *in vivo*. A-C: Levels of Fe^{2+}/Fe^{3+}, malondialdehyde, and glutathione/oxidized glutathione in renal tissues; D: Reactive oxygen species levels assessed by fluorescence microscopy in renal tissues (scale bars = 50 μm); E: Transmission electron microscopy images showing mitochondrial morphological changes related to ferroptosis in renal tissues (scale bars = 2 μm). L-KKBS: Low-dose Kunkui Baoshen decoction; H-KKBS: High-dose Kunkui Baoshen decoction; MDA: Malondialdehyde; GSH: Glutathione; GSSG: Oxidized glutathione; ROS: Reactive oxygen species. $^{b}P < 0.01$ *vs* db/m group, $^{d}P < 0.0001$ *vs* db/m group, $^{e}P < 0.05$ *vs* db/db group, $^{f}P < 0.01$ *vs* db/db group, and $^{h}P < 0.0001$ *vs* db/db group.

To determine whether KKBS inhibits HG-induced ferroptosis by modulating ferritinophagy, we used Fer-1 as a positive control. Western blot results demonstrated that HG + KKBS treatment significantly downregulated ATG7, LC3, and NCOA4 Levels while upregulating SQSTM1/p62 and FTH1 ($P < 0.05$). The HG + KKBS + Fer-1 group showed even greater suppression of ATG7, LC3, and NCOA4, along with higher SQSTM1/p62 and FTH1 Levels compared to the HG + Fer-1 group ($P < 0.05$; Figure 10I-O). Stable transfection with NCOA4 small interfering RNA effectively knocked down NCOA4 expression in HK-2 cells, with small interfering RNA3 showing the highest efficiency (Supplementary Figure 2A-C). Compared to the si-NCOA4 (NCOA4-targeting small interfering RNA) group, the si-NCOA4 + KKBS group exhibited further reductions in ATG7 and LC3 protein expression ($P < 0.05$), increased FTH1 and SLC7A11 expression ($P < 0.05$), and no significant changes in GPX4 Levels (Figure 10P-V). These findings suggest that KKBS modulates ferroptosis by regulating NCOA4-mediated ferritinophagy.

KKBS inhibits autophagy-dependent ferroptosis by enhancing the ubiquitination of NCOA4 via HERC2

As shown in Figure 10O, KKBS did not affect the mRNA levels of NCOA4, indicating that its suppression primarily occurs at the protein level without altering transcription. In eukaryotic cells, protein degradation predominantly proceeds *via* two pathways: Ubiquitin-proteasomal degradation and autophagic-lysosomal clearance[37]. To investigate the mechanism further, HK-2 cells under HG conditions were co-incubated with MG132 (a proteasome inhibitor) and 3-MA

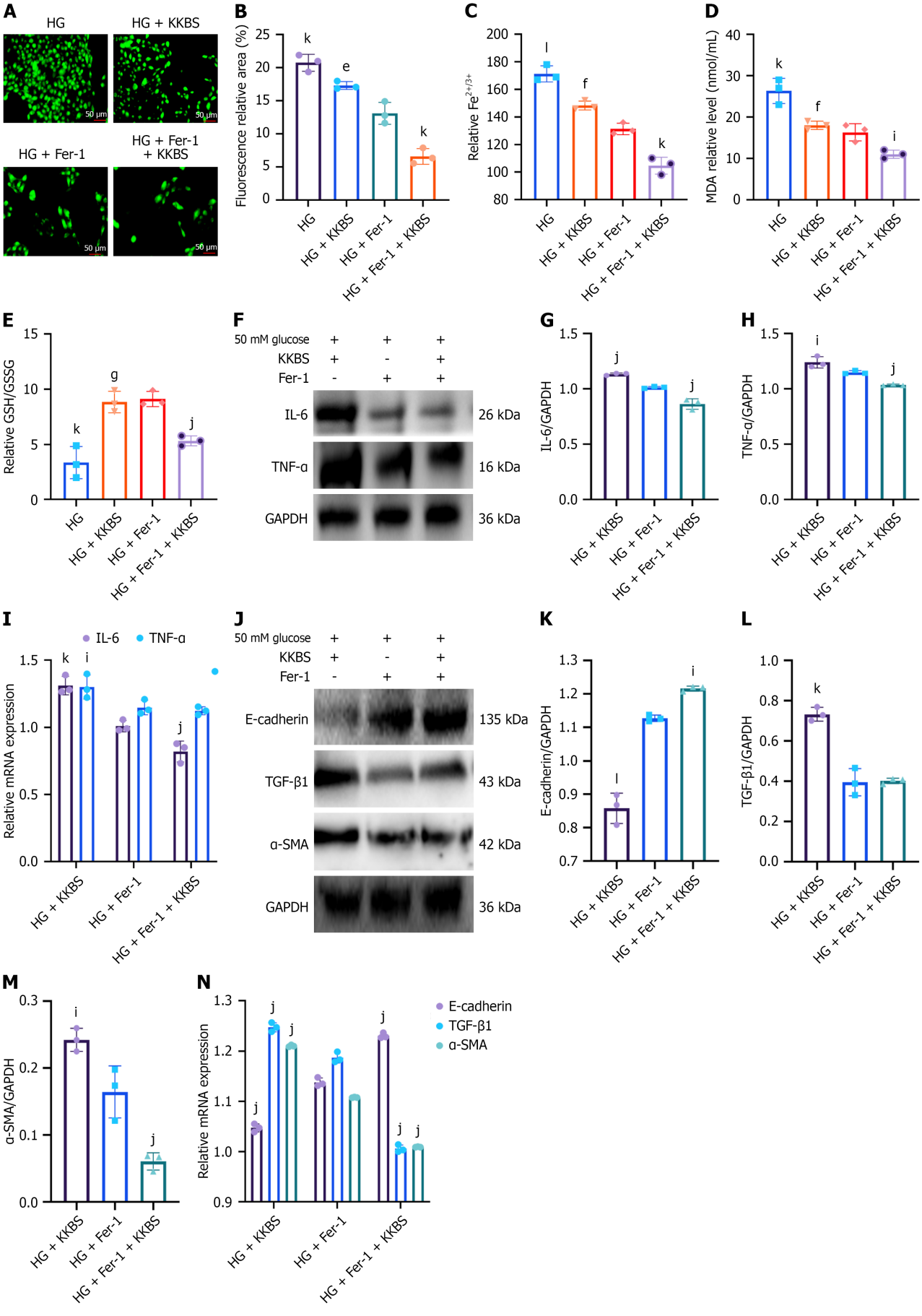


Figure 9 Kunkui Baoshen decoction alleviates fibrosis by inhibiting ferroptosis *in vitro* and *in vivo*. A and B: Reactive oxygen species expression

and fluorescence area quantification in human kidney-2 (HK-2) cells (scale bars = 50 μm); C-E: Levels of Fe^{2+}/Fe^{3+}, malondialdehyde, and glutathione/oxidized glutathione in HK-2 cells; F-I: Western blot and quantitative reverse transcription-polymerase chain reaction analyses of the inflammatory cytokines interleukin-6 and tumor necrosis factor-α in HK-2 cells; J-N: Western blot and quantitative reverse transcription-polymerase chain reaction analyses of epithelial-cadherin, α-smooth muscle actin, and transforming growth factor-β1 in HK-2 cells. KKBS: Kunkui Baoshen decoction; HG: High glucose; Fer-1: Ferrostatin-1; IL-6: Interleukin-6; TNF-α: Tumor necrosis factor-α; E-cadherin: Epithelial-cadherin; TGF-β1: Transforming growth factor-β1; α-SMA: α-smooth muscle actin; GAPDH: Glyceraldehyde 3-phosphate dehydrogenase. $^{e}P < 0.05$ *vs* high glucose group, $^{f}P < 0.01$ *vs* high glucose group, $^{g}P < 0.001$ *vs* high glucose group; $^{i}P < 0.05$ *vs* high glucose + ferrostatin-1 group, $^{j}P < 0.01$ *vs* high glucose + ferrostatin-1 group, $^{k}P < 0.001$ *vs* high glucose + ferrostatin-1 group, $^{l}P < 0.0001$ *vs* high glucose + ferrostatin-1 group.

(an autophagy inhibitor)[38]. The KKBS-induced downregulation of NCOA4 was reversed by MG132 ($P < 0.01$), but not by 3-MA (Figure 11A-D). Additionally, Co-IP assays demonstrated that KKBS markedly enhanced NCOA4 ubiquitination in HG-induced HK-2 cells, especially in the presence of MG132 (Figure 11E). These results specify that KKBS primarily reduces NCOA4 protein levels through ubiquitin-dependent proteasomal degradation.

Next, we explored the direct targets of KKBS in modulating autophagy-dependent ferroptosis in HG-induced HK-2 cells. Previous studies have shown that HERC2, an E3 ubiquitin ligase, ubiquitinates and degrades NCOA4, thereby inhibiting autophagy-dependent ferroptosis[39]. We hypothesized that KKBS might promote NCOA4 ubiquitination and degradation by upregulating HERC2 under HG conditions. Indeed, *in vitro* analyses confirmed that KKBS significantly increased HERC2 expression at both the protein ($P < 0.01$) and mRNA levels ($P < 0.001$) (Figure 11F-H). Co-IP and IF co-localization assays further validated the interaction between HERC2 and NCOA4 (Figure 11I and J).

To elucidate the functional role of HERC2 in KKBS's ferroptosis-inhibitory effects, we established an HERC2-overexpressing cell model ($P < 0.01$; Supplementary Figure 3A-C). Molecular docking of KKBS's core bioactive compounds, identified *via* LC-MS/MS, with HERC2 revealed strong binding affinities (Supplementary Figure 4A and B). Overexpression of HERC2 protected HK-2 cells from HG-induced damage ($P < 0.05$; Figure 11K and L) and led to a significant decline in NCOA4 expression ($P < 0.01$; Figure 11M-O). Moreover, co-transfection of HK-2 cells with myc-NCOA4, flag-HERC2 (F3), and histidine-ubiquitin plasmids, followed by KKBS treatment, significantly enhanced the interaction between NCOA4 and ubiquitin under HG conditions (Figure 11P).

Ubiquitin can form diverse linkages on substrates, leading to distinct cellular outcomes. To investigate the types of ubiquitin linkages involved in NCOA4 ubiquitination, we used ubiquitin mutants with lysine (K) to arginine (R) substitutions. The results showed that the ubiquitin variants K6R, K11R, K27R, K29R, K33R, and K63R increased HERC2/NCOA4 ubiquitination, whereas the K48R mutant significantly inhibited NCOA4 ubiquitination (Figure 11Q). Additionally, molecular docking analysis revealed that HERC2 (PDB ID: 7Q40) and NCOA4 (PDB ID: 1t5z) form three hydrogen bonds at residues D879-R3152, R871-R3102, and R3100-S3116, stabilizing their interaction (Figure 11R). These results imply that KKBS suppresses autophagy-dependent ferroptosis by promoting NCOA4 ubiquitination *via* HERC2.

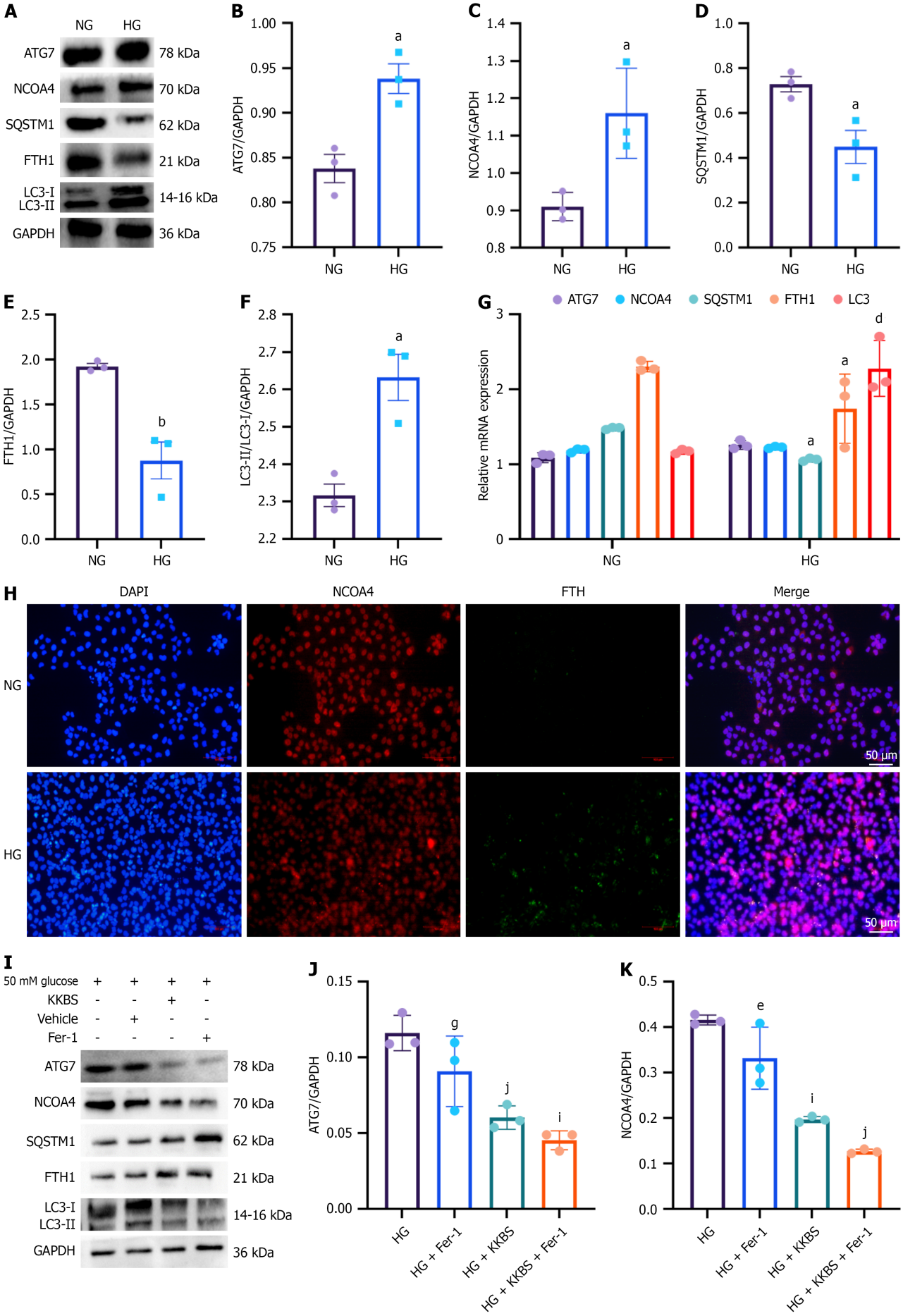
Effects of KKBS on the HERC2/NCOA4-mediated autophagy-dependent ferroptosis pathway in db/db mice

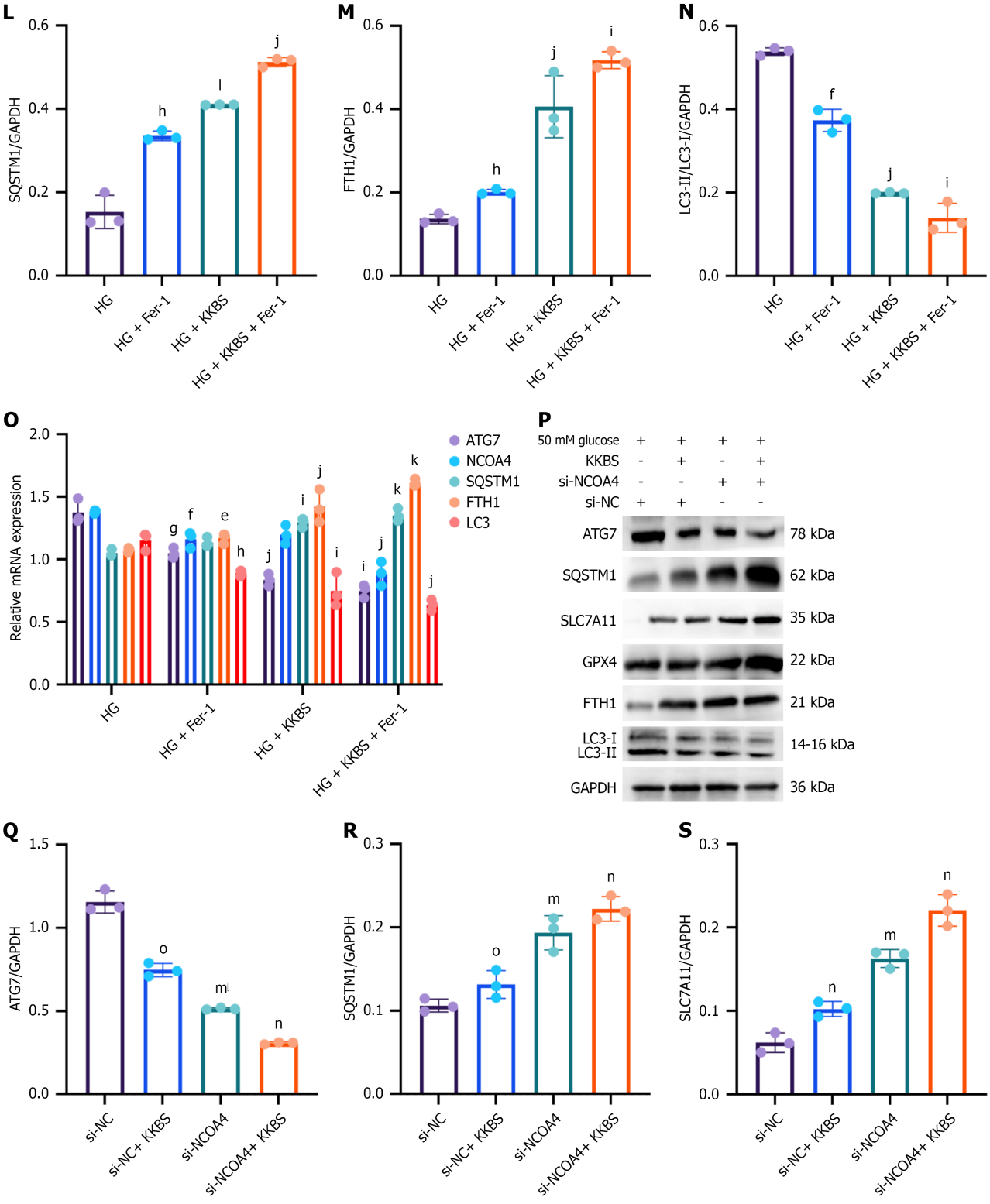
Building on the *in vitro* findings, we further examined the *in vivo* effects of KKBS on the HERC2/NCOA4-mediated autophagy-dependent ferroptosis pathway. Renal tissue expression of HERC2, NCOA4, and key ferroptosis-related autophagy markers (ATG7, SQSTM1, FTH1, LC3, SLC7A11, and GPX4) was assessed. Compared to the db/m group, the db/db group exhibited significantly elevated levels of ATG7 ($P < 0.0001$) and LC3 ($P < 0.001$), alongside reduced expression of HERC2 ($P < 0.01$), SQSTM1 ($P < 0.001$), SLC7A11 ($P < 0.01$), GPX4 ($P < 0.001$), and FTH1 ($P < 0.0001$). Treatment with KKBS significantly reversed these alterations (Figure 12A-L). Immunohistochemical staining corroborated these results (Figure 12M). Collectively, these findings indicate that KKBS alleviates renal injury by modulating the HERC2/NCOA4-mediated autophagy-dependent ferroptosis pathway in db/db mice.

DISCUSSION

DKD has emerged as a major global health priority due to its high prevalence, multiple comorbidities, significant mortality burden, and substantial economic impact. This urgent situation demands the development of improved treatment strategies and more precise, personalized diagnostic and therapeutic approaches to enhance the prevention and management of DKD[40]. In this study, LC-MS/MS analysis of KKBS identified several key quality control compounds, including secologanin, sweroside, calycosin 7-O-beta-D-glucoside, isoquercetin, quercetin, myricetin, kaempferol, ononin, and formononetin.

Metabonomic analysis revealed the GSH metabolic pathway as the most significant metabolic pathway associated with KKBS, which also represents a central metabolic feature in ferroptosis. Ferroptosis and ubiquitin-mediated proteolysis pathways are potential signaling mechanisms through which KKBS exerts therapeutic effects against DKD. Transcriptomic analysis highlighted that NCOA4 plays a substantial role in renal tubular ferroptosis in DKD. Ferritinophagy, a specialized form of autophagy mediated by NCOA4, functions as a cargo receptor that transports ferritin to lysosomes for degradation and subsequent iron release, thus maintaining cellular iron homeostasis[41,42]. Under pathological conditions such as hyperglycemia and oxidative stress, NCOA4 is upregulated and translocates to the cytoplasm, promoting ferritin recruitment to autophagosomes and triggering ferroptosis. Ferroptotic tubular epithelial cells secrete increased levels of pro-inflammatory and pro-fibrotic mediators, including TNF-α, IL-18, TGF-β1, and connective tissue growth factor, which drive renal fibrosis and contribute to DKD pathogenesis[43]. Therefore, promoting NCOA4 degradation and inhibiting autophagy-dependent ferroptosis may represent an effective strategy to prevent renal fibrosis


A
NG
HG
ATG7
78 kDa
NCOA4
70 kDa
SQSTM1
62 kDa
FTH1
21 kDa
LC3-I
LC3-II
14-16 kDa
GAPDH
36 kDa
B
ATG7/GAPDH
C
NCOA4/GAPDH
D
SQSTM1/GAPDH
E
FTH1/GAPDH
F
LC3-II/LC3-I/GAPDH
G
ATG7
NCOA4
SQSTM1
FTH1
LC3
Relative mRNA expression
H
DAPI
NCOA4
FTH
Merge
50 μm
I
50 mM glucose
KKBS
Vehicle
Fer-1
J
K
HG
HG + Fer-1
HG + KKBS
HG + KKBS + Fer-1


L
SQSTM1/GAPDH
M
FTH1/GAPDH
N
LC3-II/LC3-I/GAPDH
HG
HG + Fer-1
HG + KKBS
HG + KKBS + Fer-1
O
Relative mRNA expression
ATG7
NCOA4
SQSTM1
FTH1
LC3
P
50 mM glucose
KKBS
si-NCOA4
si-NC
ATG7
SQSTM1
SLC7A11
GPX4
FTH1
LC3-I
LC3-II
GAPDH
78 kDa
62 kDa
35 kDa
22 kDa
21 kDa
14-16 kDa
36 kDa
Q
ATG7/GAPDH
R
SQSTM1/GAPDH
S
SLC7A11/GAPDH
si-NC
si-NC+ KKBS
si-NCOA4
si-NCOA4+ KKBS

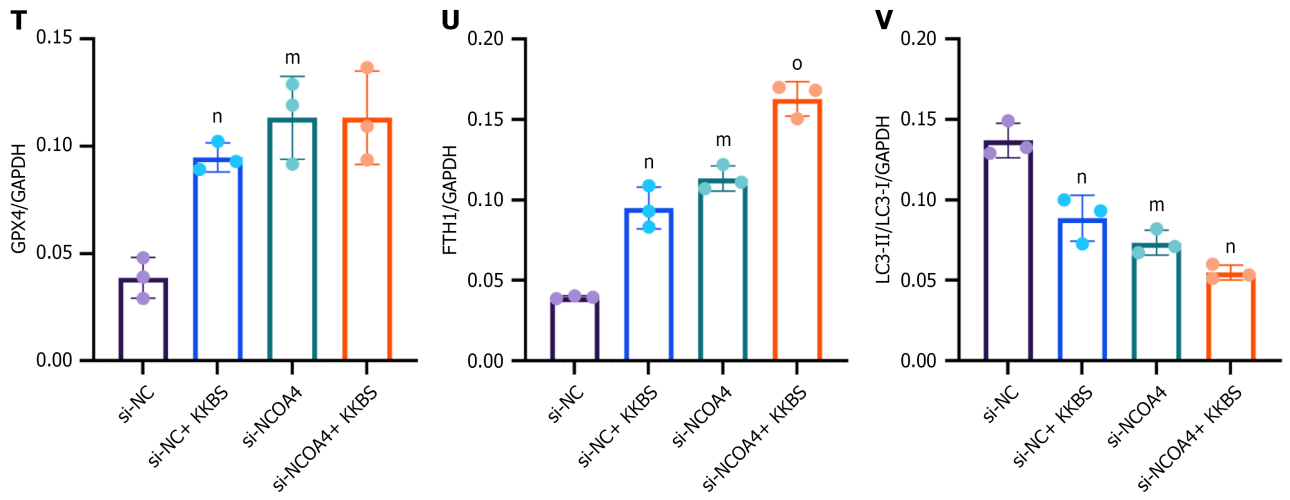


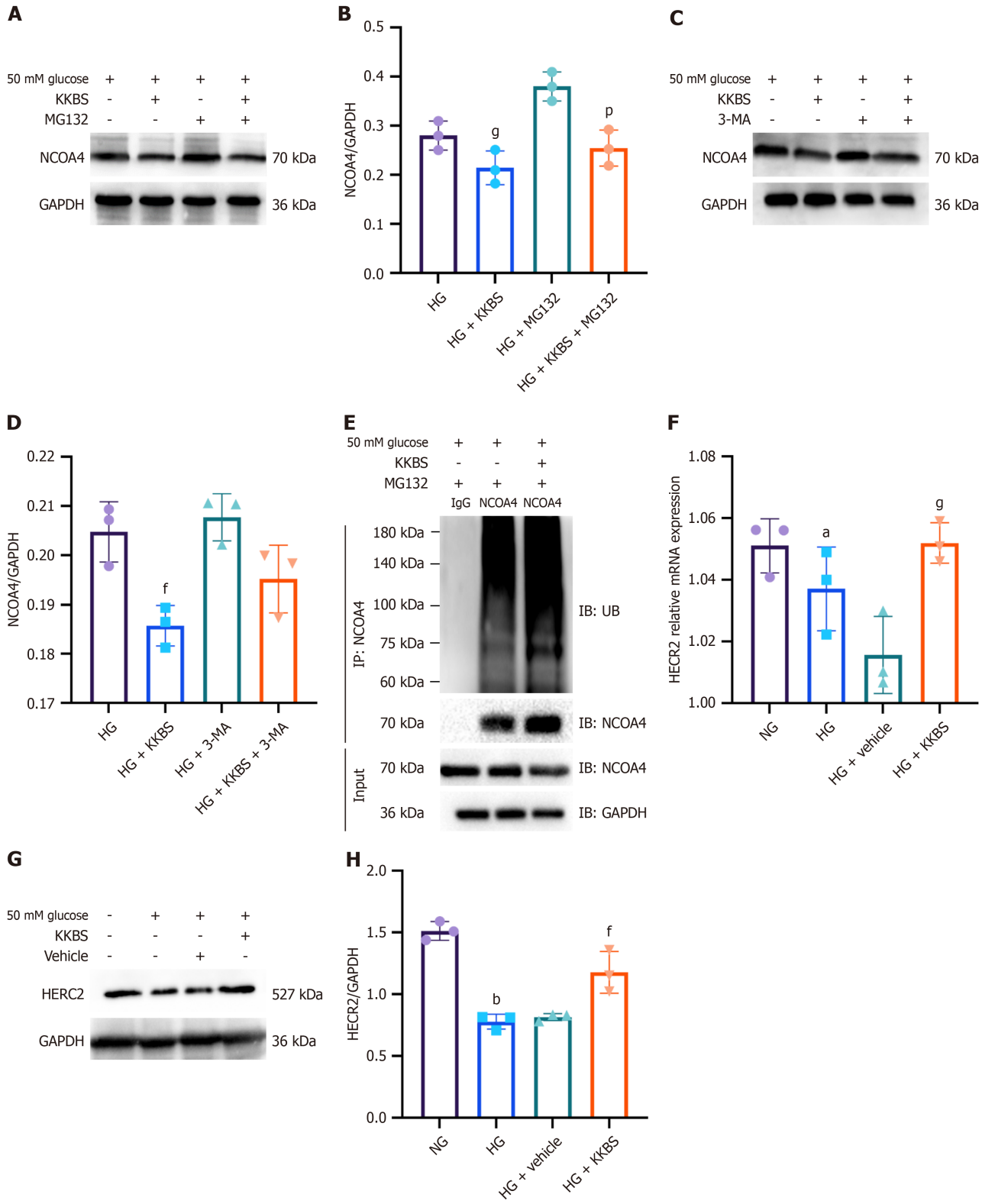
Figure 10 Kunkui Baoshen decoction modulates ferroptosis by regulating nuclear receptor coactivator 4-mediated ferritinophagy. A-G: Western blot and quantitative reverse transcription-polymerase chain reaction analyses of autophagy related 7 (ATG7), nuclear receptor coactivator 4 (NCOA4), microtubule-associated protein light chain 3 (LC3), sequestosome 1 (SQSTM1/p62), and ferritin heavy chain 1 (FTH1) in normal and high glucose groups; H: Co-localization of ferritinophagy-related proteins observed by immunofluorescence double staining in human kidney-2 cells (scale bars = 50 μm); I-O: Western blot and quantitative reverse transcription-polymerase chain reaction analyses of ATG7, NCOA4, LC3, SQSTM1/p62, and FTH1 in the four groups; P-V: Western blot analysis of ATG7, glutathione peroxidase 4, solute carrier family 7 member 11, LC3, SQSTM1/p62, and FTH1 after NCOA4 knockdown. NG: Normal group; HG: High glucose; ATG7: Autophagy related 7; NCOA4: Nuclear receptor coactivator 4; LC3: Microtubule-associated protein light chain 3; SQSTM1/p62: Sequestosome 1; FTH1: Ferritin heavy chain 1; Fer-1: Ferrostatin-1; KKBS:: Kunkui Baoshen decoction; GPX4: Glutathione peroxidase 4; SLC7A11: Solute carrier family 7 member 11; GAPDH: Glyceraldehyde 3-phosphate dehydrogenase; si-NC: Negative control small interfering RNA; si-NCOA4: Nuclear receptor coactivator 4-targeting small interfering RNA. $^{a}P < 0.05$ *vs* normal group, $^{b}P < 0.01$ *vs* normal group, $^{d}P < 0.0001$ *vs* normal group; $^{e}P < 0.05$ *vs* high glucose group, $^{f}P < 0.01$ *vs* high glucose group, $^{g}P < 0.001$ *vs* high glucose group, $^{h}P < 0.0001$ *vs* high glucose group; $^{i}P < 0.05$ *vs* high glucose + ferrostatin-1 group, $^{j}P < 0.01$ *vs* high glucose + ferrostatin-1 group, $^{k}P < 0.001$ *vs* high glucose + ferrostatin-1 group, $^{l}P < 0.0001$ *vs* high glucose + ferrostatin-1 group; $^{m}P < 0.05$ *vs* negative control small interfering RNA group; $^{n}P < 0.05$ *vs* nuclear receptor coactivator 4-targeting small interfering RNA group, and $^{o}P < 0.01$ *vs* nuclear receptor coactivator 4-targeting small interfering RNA group.

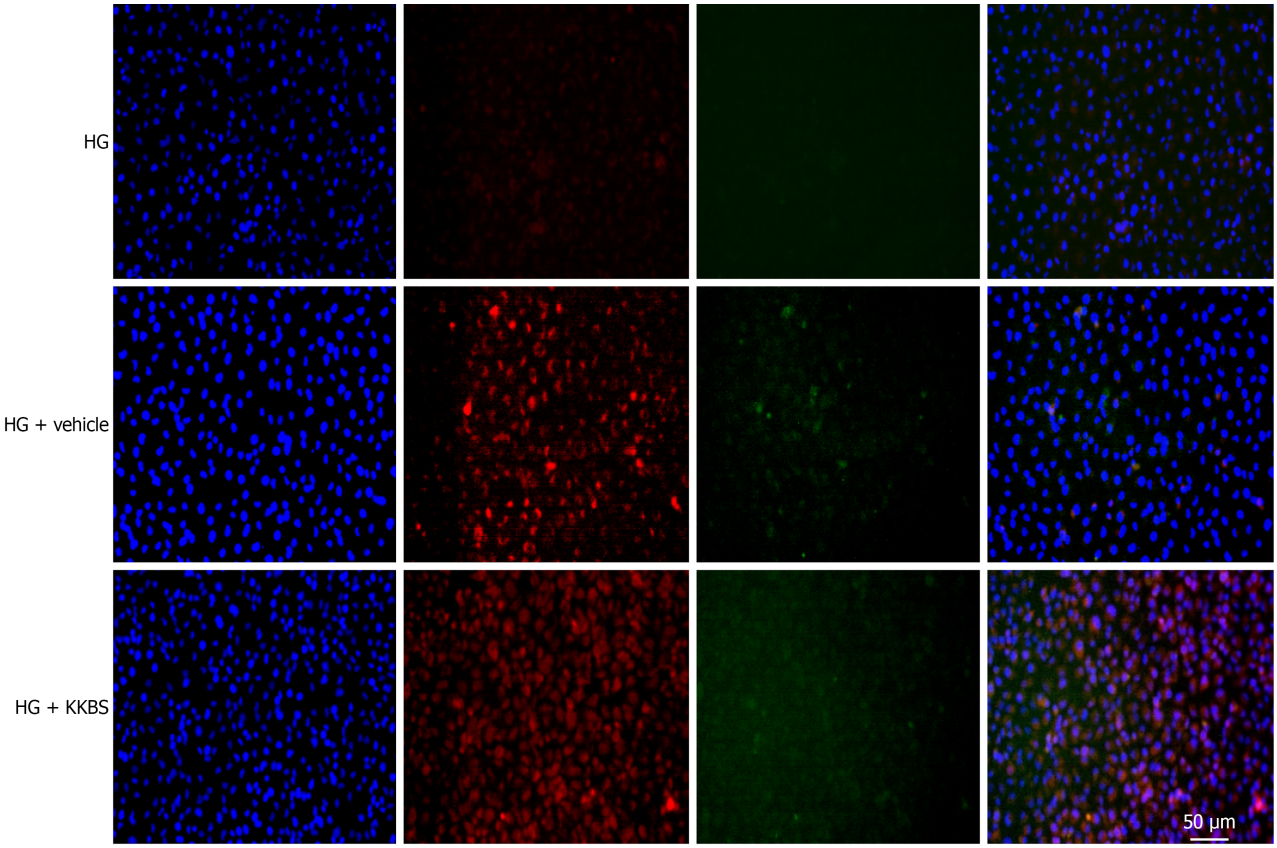
and mitigate DKD-associated damage.

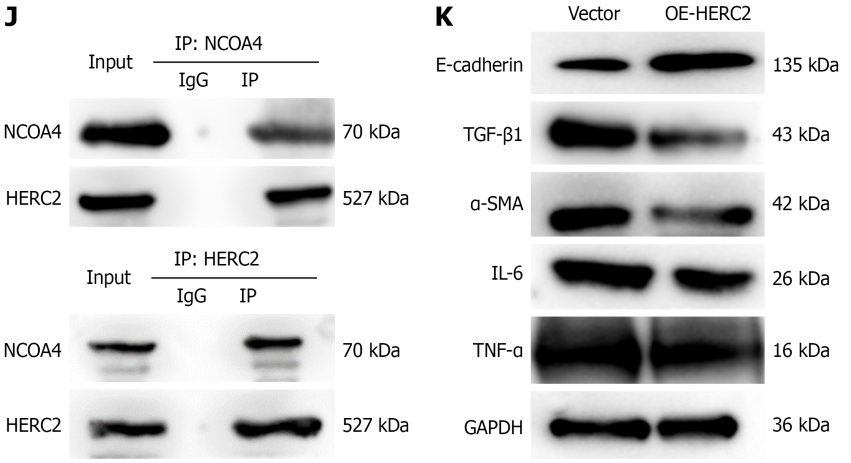
Integrating metabolomic and transcriptomic findings, the renal protective mechanisms of KKBS were investigated using HG-induced HK-2 cells and db/db mice. The results demonstrated that KKBS provides renal protection by suppressing cellular activity, migration, inflammation (IL-6 and TNF-α), the expression of fibrosis-related factors (E-cadherin, TGF-β1, and α-SMA), and apoptosis in HG-induced HK-2 cells. Elevated lipid peroxide levels and reduced GPX4 expression are two key indicators of ferroptosis[44,45], which is critically involved in the advancement of DKD-associated renal fibrosis in HG-induced HK-2 cells. KKBS mitigated HG-induced renal fibrosis by inhibiting ferroptosis-related biomarkers, including Fe^{2+}/Fe^{3+}, MDA, ROS, GSH/GSSG ratio, GPX4, and SLC7A11. We further examined the expression of autophagy markers (ATG7, SQSTM1, FTH1, and LC3) in HG-induced HK-2 cells. The data suggested that ferroptosis in these cells occurs *via* ferritinophagy, as indicated by the co-localization of NCOA4 and ferritin. Ferritinophagy is a form of selective autophagy that degrades ferritin and is primarily mediated by the cargo receptor NCOA4[46,47].

Importantly, KKBS primarily reduces NCOA4 protein levels through ubiquitin-dependent degradation. Protein ubiquitination is essential for maintaining proteostasis by regulating substrate stability[48]. This process involves a cascade of enzymes: E3 Ligases, E1 activating enzymes, and E2 conjugating enzymes, which confer substrate specificity [49,50]. Previous studies have shown that HERC2-mediated ubiquitination targets NCOA4 for proteasomal degradation, thereby inhibiting autophagy-dependent ferroptosis[51-53]. Co-IP and IF co-localization assays confirmed the interaction between HERC2 and NCOA4. To explore HERC2's role in KKBS's ferroptosis-inhibitory effects, we established an HERC2-overexpressing cell model. Overexpression of HERC2 protected HK-2 cells from HG-induced cytotoxicity and correspondingly reduced NCOA4 expression.

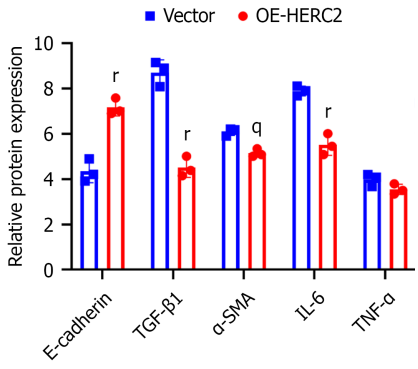
Additionally, we transfected HK-2 cells with myc-NCOA4, flag-HERC2 (F3), and His-ubiquitin constructs containing K and R mutations. The results indicated that HERC2 induces K48-linked ubiquitination, leading to NCOA4 degradation. Molecular docking simulations identified three hydrogen bonds (D879-R3152, R871-R3102, and R3100-S3116) at the HERC2-NCOA4 interface, enhancing the stability of their interaction. Next, db/db mice were employed as a DKD model to evaluate KKBS's therapeutic efficacy *in vivo*. KKBS demonstrated a favorable safety profile and alleviated renal function impairment in DKD mice. Histological assessments using HE, PAS, and Masson staining revealed that KKBS effectively protected against renal injury in db/db mice. Furthermore, Oil Red O staining showed markedly reduced lipid deposits in KKBS-treated mice compared to db/db controls, suggesting KKBS's capacity to attenuate lipid accumulation. Given that lipid peroxidation drives ferroptosis progression[54,55], these findings support the hypothesis that KKBS exerts anti-ferroptotic effects partially through lipid metabolism modulation. Finally, analyses of ferroptosis-related biomarkers *via* Western blot, TEM, and immunohistochemical demonstrated that KKBS ameliorates DKD-induced renal injury by modulating the HERC2/NCOA4-mediated autophagy-dependent ferroptosis pathway *in vivo*.

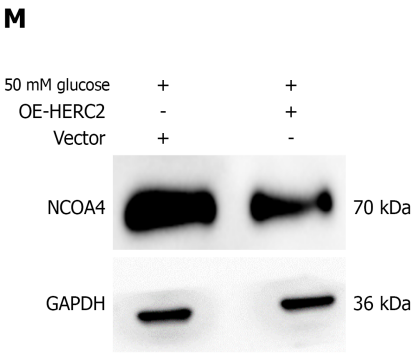

A
50 mM glucose + + + +
KKBS - + - +
MG132 - - + +
NCOA4
GAPDH
70 kDa
36 kDa
B
NCOA4/GAPDH
0.5
0.4
0.3
0.2
0.1
0.0
g
p
HG
HG + KKBS
HG + MG132
HG + KKBS + MG132
C
50 mM glucose + + + +
KKBS - + - +
3-MA - - + +
NCOA4
GAPDH
70 kDa
36 kDa
D
NCOA4/GAPDH
0.22
0.21
0.20
0.19
0.18
0.17
f
HG
HG + KKBS
HG + 3-MA
HG + KKBS + 3-MA
E
50 mM glucose + + +
KKBS - - +
MG132 + + +
IgG NCOA4 NCOA4
180 kDa
140 kDa
100 kDa
75 kDa
60 kDa
IP: NCOA4
IB: UB
70 kDa
IB: NCOA4
Input
70 kDa
IB: NCOA4
36 kDa
IB: GAPDH
F
HECR2 relative mRNA expression
1.08
1.06
1.04
1.02
1.00
a
g
NG
HG
HG + vehicle
HG + KKBS
G
50 mM glucose - + + +
KKBS - - - +
Vehicle - - + -
HERC2
GAPDH
527 kDa
36 kDa
H
HECR2/GAPDH
2.0
1.5
1.0
0.5
0.0
b
f
NG
HG
HG + vehicle
HG + KKBS
I
DAPI
HERC2
NCOA4
Merge
NG

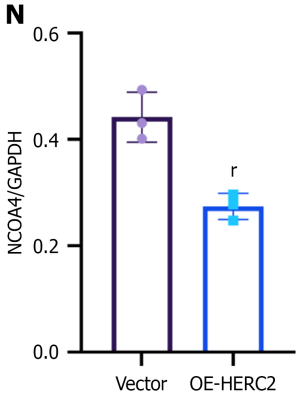

HG
HG + vehicle
HG + KKBS
50 μm

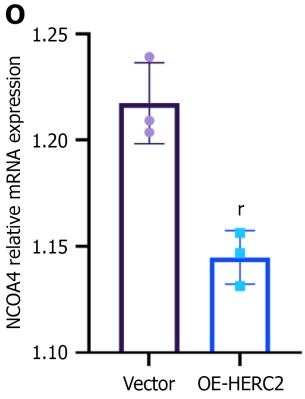

J
Input
IP: NCOA4
IgG
IP
NCOA4
70 kDa
HERC2
527 kDa
Input
IP: HERC2
IgG
IP
NCOA4
70 kDa
HERC2
527 kDa

K
Vector
OE-HERC2
E-cadherin
135 kDa
TGF-β1
43 kDa
α-SMA
42 kDa
IL-6
26 kDa
TNF-α
16 kDa
GAPDH
36 kDa


L
Vector
OE-HERC2
Relative protein expression
10
8
6
4
2
0
r
r
q
r
E-cadherin
TGF-β1
α-SMA
IL-6
TNF-α


M
50 mM glucose
+
+
OE-HERC2
-
+
Vector
+
-
NCOA4
70 kDa
GAPDH
36 kDa


N
NCOA4/GAPDH
0.6
0.4
0.2
0.0
r
Vector
OE-HERC2


O
NCOA4 relative mRNA expression
1.25
1.20
1.15
1.10
r
Vector
OE-HERC2

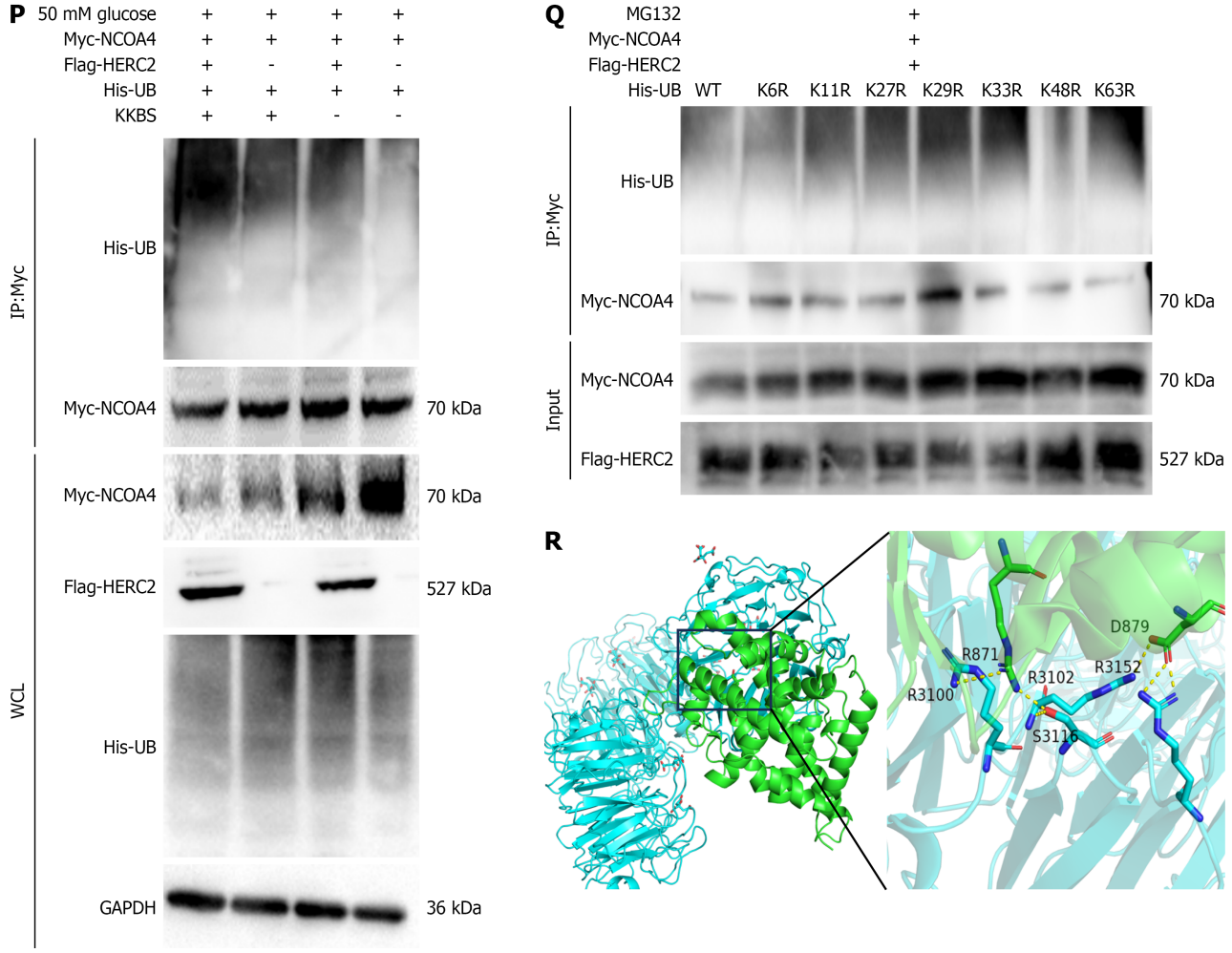
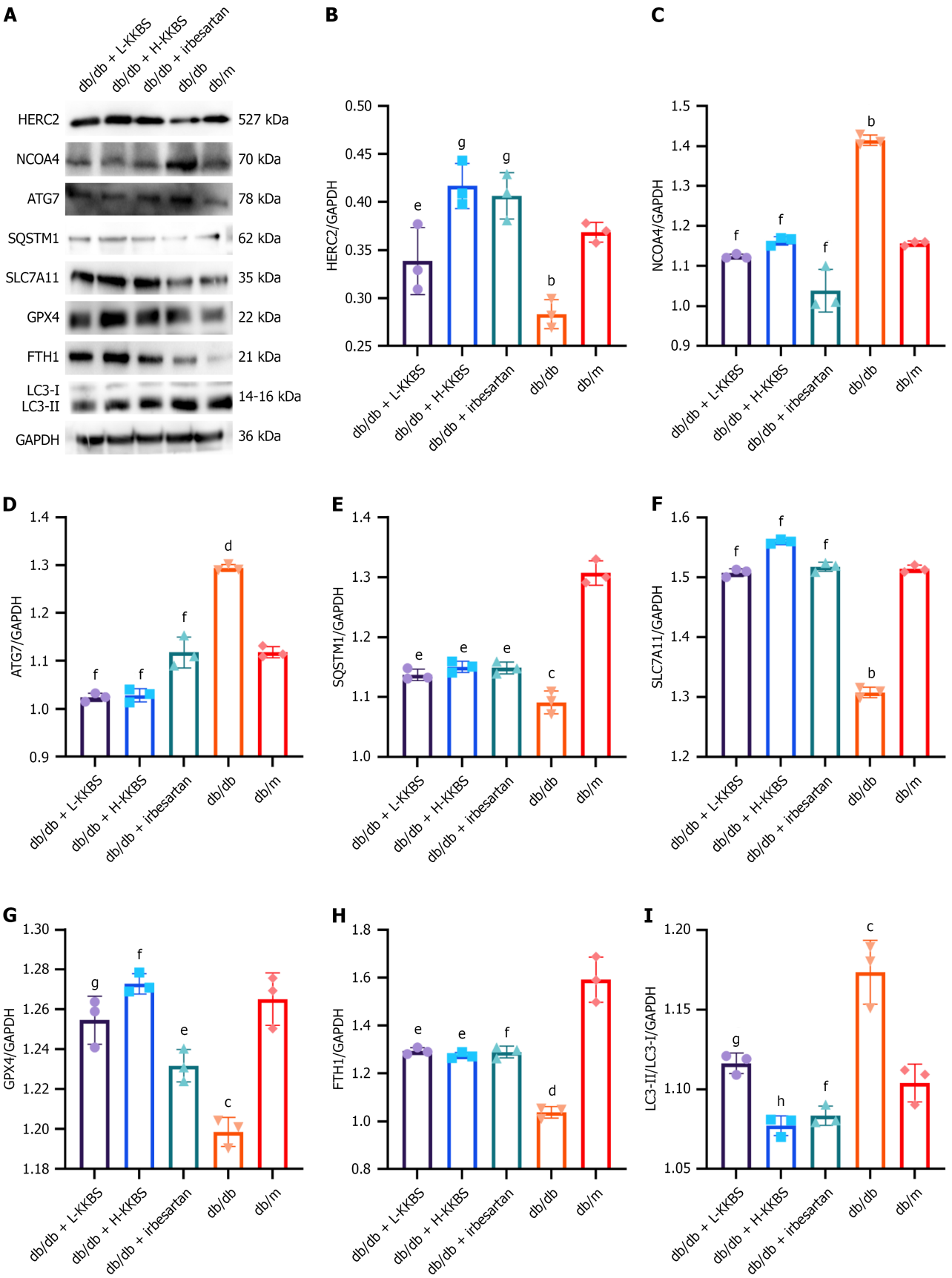


Figure 11 Kunkui Baoshen decoction inhibits autophagy-dependent ferroptosis by enhancing the ubiquitination of nuclear receptor coactivator 4 *via* homologous to E6-AP C-terminus and RCC1-like domain-containing E3 ubiquitin protein ligase. A-D: Western blot analysis of nuclear receptor coactivator 4 (NCOA4) protein levels in human kidney-2 (HK-2) cells under high glucose conditions following treatment with Kunkui Baoshen decoction (KKBS), MG132 (10 μM), and 3-MA (5 mmol/L); E: Co-immunoprecipitation was performed using NCOA4 or immunoglobulin G antibodies to evaluate NCOA4 ubiquitination in high glucose-treated HK-2 cells with or without KKBS and MG132 pretreatment. Ubiquitination levels were assessed by Western blot; F-H: KKBS significantly upregulates homologous to E6-AP C-terminus and RCC1-like domain-containing E3 ubiquitin protein ligase (HERC2) expression at both the protein and mRNA levels; I: Co-localization of NCOA4 (red) and HERC2 (green) was observed *via* immunofluorescence double staining. DAPI (blue) was used for nuclear staining (scale bars = 50 μm); J: Co-immunoprecipitation analysis was conducted using NCOA4 and HERC2 antibodies to confirm protein-protein interactions; K and L: Protein and mRNA expression levels of interleukin-6, tumor necrosis factor-α, epithelial-cadherin, α-smooth muscle actin, and transforming growth factor-β1 in HK-2 cells after HERC2 overexpression; M-O: Expression of NCOA4 following HERC2 overexpression; P: After KKBS intervention, immunoblotting of HK-2 cells was performed using His- and Myc-tag antibodies to evaluate tagged protein expression; Q: Ubiquitination assay evaluating changes in NCOA4 ubiquitination levels following ectopic transfection with different ubiquitin lysine-mutant constructs; R: Molecular docking analysis validating the interaction between HERC2 (PDB ID: 7Q40) and NCOA4 (PDB ID: 1T5Z). NCOA4: Nuclear receptor coactivator 4; HG: High glucose; KKBS: Kunkui Baoshen decoction; UB: Ubiquitin; NG: Normal group; HERC2: Homologous to E6-AP C-terminus and RCC1-like domain-containing E3 ubiquitin protein ligase; IL-6: Interleukin-6; TNF-α: Tumor necrosis factor-α; E-cadherin: Epithelial-cadherin; TGF-β1: Transforming growth factor-β1; α-SMA: α-smooth muscle actin; GAPDH: Glyceraldehyde 3-phosphate dehydrogenase; His-UB: Histidine-ubiquitin; OE-HERC2: Overexpression of homologous to E6-AP C-terminus and RCC1-like domain-containing E3 ubiquitin protein ligase. $^{a}P < 0.05$ *vs* normal group, $^{b}P < 0.01$ *vs* normal group; $^{f}P < 0.01$ *vs* high glucose group, $^{g}P < 0.001$ *vs* high glucose group; $^{g}P < 0.01$ *vs* high glucose + Kunkui Baoshen decoction group; $^{q}P < 0.05$ *vs* vector group, and $^{r}P < 0.01$ *vs* vector group.

Taken together, transcriptomic and metabolomic analyses identify ferroptosis as the central mechanism underlying KKBS's anti-renal fibrosis effects, with NCOA4 as a pivotal target. KKBS showed significant therapeutic efficacy against DKD in both cellular and animal models. Specifically, KKBS modulates the HERC2/NCOA4-mediated autophagy-dependent ferroptosis pathway, suppresses inflammatory and fibrotic factor secretion, and reduces cellular apoptosis, thereby mitigating renal damage. Furthermore, targeting the interaction between HERC2 and NCOA4 may offer a promising therapeutic strategy for DKD.

The findings align with recent studies implicating ferroptosis in the progression of DKD. For example, Tang *et al*[18] reported that enhanced ferritinophagy promotes iron overload and lipid peroxidation in DKD models, identifying NCOA4 as a critical driver of ferroptosis. Similarly, Zhou *et al*[56] highlighted the protective roles of GPX4 and SLC7A11 against oxidative stress-induced renal damage in DKD, emphasizing the therapeutic potential of targeting ferroptosis pathways. However, unlike these studies, our research uniquely identifies HERC2 as a novel upstream regulator of


A
db/db + L-KKBS
db/db + H-KKBS
db/db + irbesartan
db/db
db/m
HERC2
NCOA4
ATG7
SQSTM1
SLC7A11
GPX4
FTH1
LC3-I
LC3-II
GAPDH
527 kDa
70 kDa
78 kDa
62 kDa
35 kDa
22 kDa
21 kDa
14-16 kDa
36 kDa
B
HERC2/GAPDH
C
NCOA4/GAPDH
D
ATG7/GAPDH
E
SQSTM1/GAPDH
F
SLC7A11/GAPDH
G
GPX4/GAPDH
H
FTH1/GAPDH
I
LC3-II/LC3-I/GAPDH

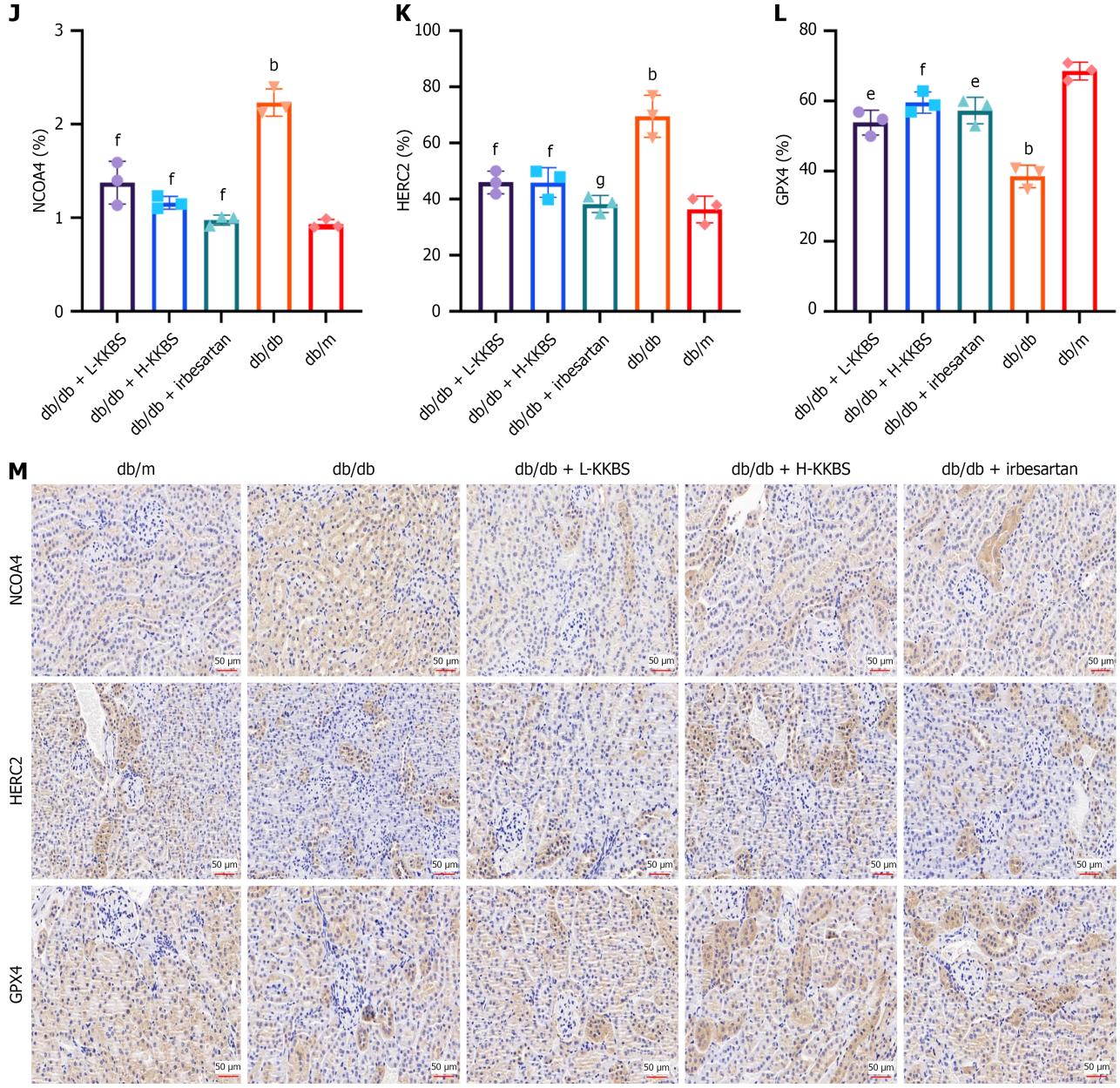


Figure 12 Effects of Kunkui Baoshen decoction on the homologous to E6-AP C-terminus and RCC1-like domain-containing E3 ubiquitin protein ligase/nuclear receptor coactivator 4-mediated autophagy-dependent ferroptosis pathway in db/db mice. A-L: Western blot analysis of key proteins involved in the homologous to E6-AP C-terminus and RCC1-like domain-containing E3 ubiquitin protein ligase/nuclear receptor coactivator 4-mediated autophagy-dependent ferroptosis pathway in db/db mice; M: Immunohistochemical staining of renal tissues showing the expression of nuclear receptor coactivator 4, homologous to E6-AP C-terminus and RCC1-like domain-containing E3 ubiquitin protein ligase, and glutathione peroxidase 4. HERC2: Homologous to E6-AP C-terminus and RCC1-like domain-containing E3 ubiquitin protein ligase; NCOA4: Nuclear receptor coactivator 4; ATG7: Autophagy related 7; SQSTM1: Sequestosome 1; SLC7A11: Solute carrier family 7 member 11; GPX4: Glutathione peroxidase 4; FTH1: Ferritin heavy chain 1; LC3: Microtubule-associated protein light chain 3; GAPDH: Glyceraldehyde 3-phosphate dehydrogenase; L-KKBS: Low-dose Kunkui Baoshen decoction; H-KKBS: High-dose Kunkui Baoshen decoction. $^{b}P < 0.01$ *vs* db/m group, $^{c}P < 0.001$ *vs* db/m group, $^{d}P < 0.0001$ *vs* db/m group; $^{e}P < 0.05$ *vs* db/db group, $^{f}P < 0.01$ *vs* db/db group, $^{g}P < 0.001$ *vs* db/db group, and $^{h}P < 0.0001$ *vs* db/db group.

NCOA4 stability *via* ubiquitin-dependent degradation, a mechanism not previously described in DKD. Moreover, whereas prior pharmacological studies have primarily focused on ferroptosis inhibitors such as Fer-1, our findings provide novel evidence supporting the use of the traditional Chinese herb KKBS to modulate ferroptosis indirectly through regulation of the autophagy machinery. This broadens the spectrum of ferroptosis-targeting therapies and highlights the therapeutic relevance of the HERC2/NCOA4 interaction as a potential druggable axis in DKD management. However, we acknowledge that our current findings mainly rely on correlative and interaction-based assays. Although the results strongly suggest a regulatory role for NCOA4 in ferroptosis *via* HERC2, we did not perform functional experiments such as NCOA4 overexpression or HERC2 knockdown/rescue assays to establish a definitive causal relationship. The absence of these validations represents a limitation of this study. Future research will focus on directly manipulating HERC2 and NCOA4 expression levels to clarify their precise roles in ferroptosis and to verify whether

Table 2 Results of liquid chromatography-mass spectrometry/mass spectrometry analysis of Kunkui Baoshen decoction

Peak name	Retention time (minutes)	Mass-to-charge ratio (experiment)	Precursor type	Compound name	Pubchem number
1	2.990916667	389.1450240	M+H	Secologanin	161276
2	3.543550000	359.1343285	M+H	Sweroside	161036
3	4.055166667	447.1292902	M+H	Calycosin 7-O-beta-D-glucoside	5318267
4	4.055166667	465.1038809	M+H	Isoquercetin	5280804
5	4.055166667	303.0504691	M+H	Quercetin	5280343
6	4.076500000	301.0350797	M+H-H_2O	Myricetin	5281672
7	4.319766667	287.0556821	M+H	Kaempferol	5280863
8	5.334866667	431.1343269	M+H	Ononin	442813
9	8.458666667	269.0813292	M+H	Formononetin	5280378

modulating this pathway can reproduce or reverse the phenotypic effects observed with KKBS treatment.

CONCLUSION

Our research provides novel evidence that KKBS exerts anti-fibrotic effects in DKD by targeting the HERC2/NCOA4-mediated autophagy-dependent ferroptosis pathway. These findings offer new mechanistic insights into DKD pathogenesis and highlight the clinical potential of modulating this pathway. KKBS's ability to ameliorate renal injury, reduce fibrosis, and regulate ferroptosis-related molecular targets, coupled with its favorable safety profile *in vivo*, establishes it as a strong contender for therapeutic development. Collectively, this research lays a theoretical groundwork for the clinical application of KKBS in DKD management and supports further translational research to evaluate its efficacy and safety in clinical settings.

ACKNOWLEDGEMENTS

We acknowledge all animals involved in this study who gave their lives for the advancement of human health.

FOOTNOTES

Author contributions: Song SY and Shan CC designed the study and contributed equally to this work as co-first authors; Zhou PP, Xu WL, and Tan Y carried out the experiments; Huang LJ, Zhou XQ, Yan QH, and Yu JY provided experiment assistance; Yu JY and Yan QH contributed equally to this work as co-corresponding authors. All authors have read and approved the final manuscript.

Supported by National Natural Science Foundation of China, No. 82205025, No. 82374355, and No. 82174293.

Institutional animal care and use committee statement: All procedures involving animals were reviewed and approved by the Institutional Animal Care and Use Committee of Affiliated Hospital of Nanjing University of Chinese Medicine, No. 2023DW-039-02.

Conflict-of-interest statement: All the authors report no relevant conflicts of interest for this article.

Data sharing statement: The raw data are available upon reasonable request from the corresponding author.

ARRIVE guidelines statement: The authors have read the ARRIVE guidelines, and the manuscript was prepared and revised according to the ARRIVE guidelines.

Open Access: This article is an open-access article that was selected by an in-house editor and fully peer-reviewed by external reviewers. It is distributed in accordance with the Creative Commons Attribution NonCommercial (CC BY-NC 4.0) license, which permits others to distribute, remix, adapt, build upon this work non-commercially, and license their derivative works on different terms, provided the original work is properly cited and the use is non-commercial. See: https://creativecommons.org/Licenses/by-nc/4.0/

Country of origin: China

ORCID number: Ying Tan 0000-0002-7419-0762; Jiang-Yi Yu 0000-0001-7159-5396.

S-Editor: Wu S
L-Editor: Wang TQ
P-Editor: Xu ZH

REFERENCES

1 **Mohandes S**, Doke T, Hu H, Mukhi D, Dhillon P, Susztak K. Molecular pathways that drive diabetic kidney disease. *J Clin Invest* 2023; **133**: e165654 [*RCA*] [PMID: 36787250 DOI: 10.1172/JCI165654] [FullText] [Full Text(PDF)]
2 **Xue X**, Jin XY, Ye XL, Li KY, Li JX, Liu XH, Bai J, Liu Q, Zhang BR, Zou XR, Yuan J, Lu CL, Zhao FF, Liu JP, Wang XQ. Ophiocordyceps sinensis preparations combined with the renin-angiotensin system inhibitor for diabetic kidney disease treatment: an umbrella review of systematic reviews and network meta-analysis. *Front Pharmacol* 2024; **15**: 1360633 [*RCA*] [PMID: 38716236 DOI: 10.3389/fphar.2024.1360633] [FullText] [Full Text(PDF)]
3 **Wang Y**, Quan F, Cao Q, Lin Y, Yue C, Bi R, Cui X, Yang H, Yang Y, Birnbaumer L, Li X, Gao X. Quercetin alleviates acute kidney injury by inhibiting ferroptosis. *J Adv Res* 2021; **28**: 231-243 [*RCA*] [PMID: 33364059 DOI: 10.1016/j.jare.2020.07.007] [FullText] [Full Text(PDF)]
4 **Xie D**, Esmaiel H, Sun H, Qi J, Qasem ZAH. Feature Extraction of Ship-Radiated Noise Based on Enhanced Variational Mode Decomposition, Normalized Correlation Coefficient and Permutation Entropy. *Entropy (Basel)* 2020; **22**: 468 [*RCA*] [PMID: 33286242 DOI: 10.3390/e22040468] [FullText] [Full Text(PDF)]
5 **Song S**, Yu J. Integrating Network Pharmacology, Bioinformatics, and Mendelian Randomization Analysis to Identify Hub Targets and Mechanisms of Kunkui Baoshen Decoction in Treating Diabetic Kidney Disease. *Curr Pharm Des* 2024; **30**: 3367-3393 [*RCA*] [PMID: 39238373 DOI: 10.2174/0113816128331463240816145054] [FullText]
6 **Wei C**, Wang C, Li R, Bai Y, Wang X, Fang Q, Chen X, Li P. The pharmacological mechanism of Abelmoschus manihot in the treatment of chronic kidney disease. *Heliyon* 2023; **9**: e22017 [*RCA*] [PMID: 38058638 DOI: 10.1016/j.heliyon.2023.e22017] [FullText] [Full Text(PDF)]
7 **Tan Y**, Li R, Zhou P, Li N, Xu W, Zhou X, Yan Q, Yu J. Huobahuagen tablet improves renal function in diabetic kidney disease: a real-world retrospective cohort study. *Front Endocrinol (Lausanne)* 2023; **14**: 1166880 [*RCA*] [PMID: 37404303 DOI: 10.3389/fendo.2023.1166880] [FullText]
8 **Han H**, Cao A, Wang L, Guo H, Zang Y, Li Z, Zhang X, Peng W. Huangqi Decoction Ameliorates Streptozotocin-Induced Rat Diabetic Nephropathy through Antioxidant and Regulation of the TGF-β/MAPK/PPAR-γ Signaling. *Cell Physiol Biochem* 2017; **42**: 1934-1944 [*RCA*] [PMID: 28793292 DOI: 10.1159/000479834] [FullText]
9 **Xu H**, Shen J, Liu H, Shi Y, Li L, Wei M. Morroniside and loganin extracted from Cornus officinalis have protective effects on rat mesangial cell proliferation exposed to advanced glycation end products by preventing oxidative stress. *Can J Physiol Pharmacol* 2006; **84**: 1267-1273 [*RCA*] [PMID: 17487235 DOI: 10.1139/y06-075] [FullText]
10 **Dixon SJ**, Lemberg KM, Lamprecht MR, Skouta R, Zaitsev EM, Gleason CE, Patel DN, Bauer AJ, Cantley AM, Yang WS, Morrison B 3rd, Stockwell BR. Ferroptosis: an iron-dependent form of nonapoptotic cell death. *Cell* 2012; **149**: 1060-1072 [*RCA*] [PMID: 22632970 DOI: 10.1016/j.cell.2012.03.042] [FullText]
11 **Fang X**, Ardehali H, Min J, Wang F. The molecular and metabolic landscape of iron and ferroptosis in cardiovascular disease. *Nat Rev Cardiol* 2023; **20**: 7-23 [*RCA*] [PMID: 35788564 DOI: 10.1038/s41569-022-00735-4] [FullText] [Full Text(PDF)]
12 **Liang D**, Minikes AM, Jiang X. Ferroptosis at the intersection of lipid metabolism and cellular signaling. *Mol Cell* 2022; **82**: 2215-2227 [*RCA*] [PMID: 35390277 DOI: 10.1016/j.molcel.2022.03.022] [FullText]
13 **Wu X**, Li Y, Zhang S, Zhou X. Ferroptosis as a novel therapeutic target for cardiovascular disease. *Theranostics* 2021; **11**: 3052-3059 [*RCA*] [PMID: 33537073 DOI: 10.7150/thno.54113] [FullText] [Full Text(PDF)]
14 **Doll S**, Freitas FP, Shah R, Aldrovandi M, da Silva MC, Ingold I, Goya Grocin A, Xavier da Silva TN, Panzilius E, Scheel CH, Mourão A, Buday K, Sato M, Wanninger J, Vignane T, Mohana V, Rehberg M, Flatley A, Schepers A, Kurz A, White D, Sauer M, Sattler M, Tate EW, Schmitz W, Schulze A, O'Donnell V, Proneth B, Popowicz GM, Pratt DA, Angeli JPF, Conrad M. FSP1 is a glutathione-independent ferroptosis suppressor. *Nature* 2019; **575**: 693-698 [*RCA*] [PMID: 31634899 DOI: 10.1038/s41586-019-1707-0] [FullText]
15 **Ji H**, Wang W, Li X, Han X, Zhang X, Wang J, Liu C, Huang L, Gao W. p53: A double-edged sword in tumor ferroptosis. *Pharmacol Res* 2022; **177**: 106013 [*RCA*] [PMID: 34856333 DOI: 10.1016/j.phrs.2021.106013] [FullText]
16 **Kraft VAN**, Bezjian CT, Pfeiffer S, Ringelstetter L, Müller C, Zandkarimi F, Merl-Pham J, Bao X, Anastasov N, Kössl J, Brandner S, Daniels JD, Schmitt-Kopplin P, Hauck SM, Stockwell BR, Hadian K, Schick JA. GTP Cyclohydrolase 1/Tetrahydrobiopterin Counteract Ferroptosis through Lipid Remodeling. *ACS Cent Sci* 2020; **6**: 41-53 [*RCA*] [PMID: 31989025 DOI: 10.1021/acscentsci.9b01063] [FullText] [Full Text(PDF)]
17 **Jiang X**, Stockwell BR, Conrad M. Ferroptosis: mechanisms, biology and role in disease. *Nat Rev Mol Cell Biol* 2021; **22**: 266-282 [*RCA*] [PMID: 33495651 DOI: 10.1038/s41580-020-00324-8] [FullText]
18 **Tang D**, Chen X, Kang R, Kroemer G. Ferroptosis: molecular mechanisms and health implications. *Cell Res* 2021; **31**: 107-125 [*RCA*] [PMID: 33268902 DOI: 10.1038/s41422-020-00441-1] [FullText] [Full Text(PDF)]
19 **Feng Q**, Yang Y, Qiao Y, Zheng Y, Yu X, Liu F, Wang H, Zheng B, Pan S, Ren K, Liu D, Liu Z. Quercetin Ameliorates Diabetic Kidney Injury by Inhibiting Ferroptosis *via* Activating Nrf2/HO-1 Signaling Pathway. *Am J Chin Med* 2023; **51**: 997-1018 [*RCA*] [PMID: 37046368 DOI: 10.1142/S0192415X23500465] [FullText]
20 **Wang L**, Wu J, Wang Y. The Prevalence and Treatment of Diabetes in China From 2013 to 2018-Reply. *JAMA* 2022; **327**: 1706-1707 [*RCA*] [PMID: 35503349 DOI: 10.1001/jama.2022.3017] [FullText]
21 **Alam MA**, Al-Jenoobi FI, Al-Mohizea AM. Everted gut sac model as a tool in pharmaceutical research: limitations and applications. *J Pharm Pharmacol* 2012; **64**: 326-336 [*RCA*] [PMID: 22309264 DOI: 10.1111/j.2042-7158.2011.01391.x] [FullText]
22 **Bian Y**, Gao C, Kuster B. On the potential of micro-flow LC-MS/MS in proteomics. *Expert Rev Proteomics* 2022; **19**: 153-164 [*RCA*] [PMID: 36221222 DOI: 10.1080/14789450.2022.2134780] [FullText]

23 **Wishart DS**, Guo A, Oler E, Wang F, Anjum A, Peters H, Dizon R, Sayeeda Z, Tian S, Lee BL, Berjanskii M, Mah R, Yamamoto M, Jovel J, Torres-Calzada C, Hiebert-Giesbrecht M, Lui VW, Varshavi D, Varshavi D, Allen D, Arndt D, Khetarpal N, Sivakumaran A, Harford K, Sanford S, Yee K, Cao X, Budinski Z, Liigand J, Zhang L, Zheng J, Mandal R, Karu N, Dambrova M, Schiöth HB, Greiner R, Gautam V. HMDB 5.0: the Human Metabolome Database for 2022. *Nucleic Acids Res* 2022; **50**: D622-D631 [*RCA*] [PMID: 34986597 DOI: 10.1093/nar/gkab1062] [FullText] [Full Text(PDF)]

24 **Baker ES**, Hoang C, Uritboonthai W, Heyman HM, Pratt B, MacCoss M, MacLean B, Plumb R, Aisporna A, Siuzdak G. METLIN-CCS: an ion mobility spectrometry collision cross section database. *Nat Methods* 2023; **20**: 1836-1837 [*RCA*] [PMID: 37932399 DOI: 10.1038/s41592-023-02078-5] [FullText]

25 **Ren Y**, Yu G, Shi C, Liu L, Guo Q, Han C, Zhang D, Zhang L, Liu B, Gao H, Zeng J, Zhou Y, Qiu Y, Wei J, Luo Y, Zhu F, Li X, Wu Q, Li B, Fu W, Tong Y, Meng J, Fang Y, Dong J, Feng Y, Xie S, Yang Q, Yang H, Wang Y, Zhang J, Gu H, Xuan H, Zou G, Luo C, Huang L, Yang B, Dong Y, Zhao J, Han J, Zhang X, Huang H. Majorbio Cloud: A one-stop, comprehensive bioinformatic platform for multiomics analyses. *Imeta* 2022; **1**: e12 [*RCA*] [PMID: 38868573 DOI: 10.1002/imt2.12] [FullText] [Full Text(PDF)]

26 **Kanehisa M**, Goto S. KEGG: kyoto encyclopedia of genes and genomes. *Nucleic Acids Res* 2000; **28**: 27-30 [*RCA*] [PMID: 10592173 DOI: 10.1093/nar/28.1.27] [FullText]

27 **Karuppasamy MP**, Venkateswaran S, Subbiah P. PDB-2-PBv3.0: An updated protein block database. *J Bioinform Comput Biol* 2020; **18**: 2050009 [*RCA*] [PMID: 32404014 DOI: 10.1142/S0219720020500092] [FullText]

28 **Forli S**, Huey R, Pique ME, Sanner MF, Goodsell DS, Olson AJ. Computational protein-ligand docking and virtual drug screening with the AutoDock suite. *Nat Protoc* 2016; **11**: 905-919 [*RCA*] [PMID: 27077332 DOI: 10.1038/nprot.2016.051] [FullText]

29 **Love MI**, Huber W, Anders S. Moderated estimation of fold change and dispersion for RNA-seq data with DESeq2. *Genome Biol* 2014; **15**: 550 [*RCA*] [PMID: 25516281 DOI: 10.1186/s13059-014-0550-8] [FullText] [Full Text(PDF)]

30 **Kanehisa M**, Araki M, Goto S, Hattori M, Hirakawa M, Itoh M, Katayama T, Kawashima S, Okuda S, Tokimatsu T, Yamanishi Y. KEGG for linking genomes to life and the environment. *Nucleic Acids Res* 2008; **36**: D480-D484 [*RCA*] [PMID: 18077471 DOI: 10.1093/nar/gkm882] [FullText] [Full Text(PDF)]

31 **Tesch GH**, Lim AK. Recent insights into diabetic renal injury from the db/db mouse model of type 2 diabetic nephropathy. *Am J Physiol Renal Physiol* 2011; **300**: F301-F310 [*RCA*] [PMID: 21147843 DOI: 10.1152/ajprenal.00607.2010] [FullText]

32 **Ni B**, Xiao Y, Wei R, Liu W, Zhu L, Liu Y, Ruan Z, Li J, Wang S, Zhao J, Huang W. Qufeng tongluo decoction decreased proteinuria in diabetic mice by protecting podocytes *via* promoting autophagy. *J Tradit Complement Med* 2024; **14**: 312-320 [*RCA*] [PMID: 38707926 DOI: 10.1016/j.jtcme.2023.11.007] [FullText] [Full Text(PDF)]

33 **Cui Y**, Yu L, Cong W, Jiang S, Qiu X, Wei C, Zheng G, Mao J, Liu R, Patzak A, Persson PB, Chen J, Zhao L, Lai EY. Irisin preserves mitochondrial integrity and function in tubular epithelial cells after ischemia-reperfusion-induced acute kidney injury. *Acta Physiol (Oxf)* 2024; **240**: e14211 [*RCA*] [PMID: 39073055 DOI: 10.1111/apha.14211] [FullText]

34 **Zheng J**, Conrad M. Ferroptosis: when metabolism meets cell death. *Physiol Rev* 2025; **105**: 651-706 [*RCA*] [PMID: 39661331 DOI: 10.1152/physrev.00031.2024] [FullText]

35 **Wei S**, Qiu T, Yao X, Wang N, Jiang L, Jia X, Tao Y, Wang Z, Pei P, Zhang J, Zhu Y, Yang G, Liu X, Liu S, Sun X. Arsenic induces pancreatic dysfunction and ferroptosis *via* mitochondrial ROS-autophagy-lysosomal pathway. *J Hazard Mater* 2020; **384**: 121390 [*RCA*] [PMID: 31735470 DOI: 10.1016/j.jhazmat.2019.121390] [FullText]

36 **Fang Y**, Chen X, Tan Q, Zhou H, Xu J, Gu Q. Inhibiting Ferroptosis through Disrupting the NCOA4-FTH1 Interaction: A New Mechanism of Action. *ACS Cent Sci* 2021; **7**: 980-989 [*RCA*] [PMID: 34235259 DOI: 10.1021/acscentsci.0c01592] [FullText] [Full Text(PDF)]

37 **Raffeiner M**, Zhu S, González-Fuente M, Üstün S. Interplay between autophagy and proteasome during protein turnover. *Trends Plant Sci* 2023; **28**: 698-714 [*RCA*] [PMID: 36801193 DOI: 10.1016/j.tplants.2023.01.013] [FullText]

38 **Chen Y**, Shen J, Yuan M, Li H, Li Y, Zheng S, Han B, Zhang C, Liu S, Sun Q, Wu J. Dehydrocostus lactone suppresses gastric cancer progression by targeting ACLY to inhibit fatty acid synthesis and autophagic flux. *J Adv Res* 2025; **67**: 331-348 [*RCA*] [PMID: 38295877 DOI: 10.1016/j.jare.2024.01.028] [FullText]

39 **Anandhan A**, Dodson M, Shakya A, Chen J, Liu P, Wei Y, Tan H, Wang Q, Jiang Z, Yang K, Garcia JG, Chambers SK, Chapman E, Ooi A, Yang-Hartwich Y, Stockwell BR, Zhang DD. NRF2 controls iron homeostasis and ferroptosis through HERC2 and VAMP8. *Sci Adv* 2023; **9**: eade9585 [*RCA*] [PMID: 36724221 DOI: 10.1126/sciadv.ade9585] [FullText] [Full Text(PDF)]

40 **Wang H**, Yu X, Liu D, Qiao Y, Huo J, Pan S, Zhou L, Wang R, Feng Q, Liu Z. VDR Activation Attenuates Renal Tubular Epithelial Cell Ferroptosis by Regulating Nrf2/HO-1 Signaling Pathway in Diabetic Nephropathy. *Adv Sci (Weinh)* 2024; **11**: e2305563 [*RCA*] [PMID: 38145959 DOI: 10.1002/advs.202305563] [FullText] [Full Text(PDF)]

41 **Ma J**, Chen S, Liu J, Liao Y, Li L, Wang CC, Song S, Feng R, Hu H, Quan S. Cryptochrome 1 regulates ovarian granulosa cell senescence through NCOA4-mediated ferritinophagy. *Free Radic Biol Med* 2024; **217**: 1-14 [*RCA*] [PMID: 38522484 DOI: 10.1016/j.freeradbiomed.2024.03.015] [FullText]

42 **Qin Y**, Qiao Y, Wang D, Tang C, Yan G. Ferritinophagy and ferroptosis in cardiovascular disease: Mechanisms and potential applications. *Biomed Pharmacother* 2021; **141**: 111872 [*RCA*] [PMID: 34246187 DOI: 10.1016/j.biopha.2021.111872] [FullText]

43 **Han Z**, Luo Y, Chen H, Zhang G, You L, Zhang M, Lin Y, Yuan L, Zhou S. A Deep Insight into Ferroptosis in Renal Disease: Facts and Perspectives. *Kidney Dis (Basel)* 2024; **10**: 224-236 [*RCA*] [PMID: 38835406 DOI: 10.1159/000538106] [FullText]

44 **Dai E**, Han L, Liu J, Xie Y, Kroemer G, Klionsky DJ, Zeh HJ, Kang R, Wang J, Tang D. Autophagy-dependent ferroptosis drives tumor-associated macrophage polarization *via* release and uptake of oncogenic KRAS protein. *Autophagy* 2020; **16**: 2069-2083 [*RCA*] [PMID: 31920150 DOI: 10.1080/15548627.2020.1714209] [FullText]

45 **Tang M**, Chen Z, Wu D, Chen L. Ferritinophagy/ferroptosis: Iron-related newcomers in human diseases. *J Cell Physiol* 2018; **233**: 9179-9190 [*RCA*] [PMID: 30076709 DOI: 10.1002/jcp.26954] [FullText]

46 **Mancias JD**, Wang X, Gygi SP, Harper JW, Kimmelman AC. Quantitative proteomics identifies NCOA4 as the cargo receptor mediating ferritinophagy. *Nature* 2014; **509**: 105-109 [*RCA*] [PMID: 24695223 DOI: 10.1038/nature13148] [FullText] [Full Text(PDF)]

47 **Santana-Codina N**, Gikandi A, Mancias JD. The Role of NCOA4-Mediated Ferritinophagy in Ferroptosis. *Adv Exp Med Biol* 2021; **1301**: 41-57 [*RCA*] [PMID: 34370287 DOI: 10.1007/978-3-030-62026-4_4] [FullText]

48 **Ji YX**, Zhang P, Zhang XJ, Zhao YC, Deng KQ, Jiang X, Wang PX, Huang Z, Li H. The ubiquitin E3 ligase TRAF6 exacerbates pathological cardiac hypertrophy *via* TAK1-dependent signalling. *Nat Commun* 2016; **7**: 11267 [*RCA*] [PMID: 27249171 DOI: 10.1038/ncomms11267] [FullText] [Full Text(PDF)]

49 **Rong Y**, Fan J, Ji C, Wang Z, Ge X, Wang J, Ye W, Yin G, Cai W, Liu W. USP11 regulates autophagy-dependent ferroptosis after spinal cord ischemia-reperfusion injury by deubiquitinating Beclin 1. *Cell Death Differ* 2022; **29**: 1164-1175 [*RCA*] [PMID: 34839355 DOI: 10.1038/s41418-021-00907-8] [FullText]

50 **Tyagi A**, Haq S, Ramakrishna S. Redox regulation of DUBs and its therapeutic implications in cancer. *Redox Biol* 2021; **48**: 102194 [*RCA*] [PMID: 34814083 DOI: 10.1016/j.redox.2021.102194] [FullText] [Full Text(PDF)]

51 **Ma F**, Shao X, Zhang Y, Li J, Li Q, Sun H, Wang T, Liu H, Zhao F, Chen L, Chen J, Zhou S, Ji Q, Yu P. An arterial spin labeling-based radiomics signature and machine learning for the prediction and detection of various stages of kidney damage due to diabetes. *Front Endocrinol (Lausanne)* 2024; **15**: 1333881 [*RCA*] [PMID: 39624821 DOI: 10.3389/fendo.2024.1333881] [FullText]

52 **Mancias JD**, Pontano Vaites L, Nissim S, Biancur DE, Kim AJ, Wang X, Liu Y, Goessling W, Kimmelman AC, Harper JW. Ferritinophagy *via* NCOA4 is required for erythropoiesis and is regulated by iron dependent HERC2-mediated proteolysis. *Elife* 2015; **4**: e10308 [*RCA*] [PMID: 26436293 DOI: 10.7554/eLife.10308] [FullText] [Full Text(PDF)]

53 **Zhang SJ**, Zhang YF, Bai XH, Zhou MQ, Zhang ZY, Zhang SX, Cao ZJ, Wang L, Ding SW, Zheng HJ, Liu YN, Yu GY, Liu WJ. Integrated Network Pharmacology Analysis and Experimental Validation to Elucidate the Mechanism of Acteoside in Treating Diabetic Kidney Disease. *Drug Des Devel Ther* 2024; **18**: 1439-1457 [*RCA*] [PMID: 38707616 DOI: 10.2147/DDDT.S445254] [FullText] [Full Text(PDF)]

54 **Bell HN**, Stockwell BR, Zou W. Ironing out the role of ferroptosis in immunity. *Immunity* 2024; **57**: 941-956 [*RCA*] [PMID: 38749397 DOI: 10.1016/j.immuni.2024.03.019] [FullText] [Full Text(PDF)]

55 **Ursini F**, Maiorino M. Lipid peroxidation and ferroptosis: The role of GSH and GPx4. *Free Radic Biol Med* 2020; **152**: 175-185 [*RCA*] [PMID: 32165281 DOI: 10.1016/j.freeradbiomed.2020.02.027] [FullText]

56 **Zhou H**, Zhou YL, Mao JA, Tang LF, Xu J, Wang ZX, He Y, Li M. NCOA4-mediated ferritinophagy is involved in ionizing radiation-induced ferroptosis of intestinal epithelial cells. *Redox Biol* 2022; **55**: 102413 [*RCA*] [PMID: 35932693 DOI: 10.1016/j.redox.2022.102413] [FullText] [Full Text(PDF)]

Published by **Baishideng Publishing Group Inc**
7041 Koll Center Parkway, Suite 160, Pleasanton, CA 94566, USA
Telephone: +1-925-3991568
E-mail: office@baishideng.com
Help Desk: https://www.f6publishing.com/helpdesk
https://www.wjgnet.com

© 2025 Baishideng Publishing Group Inc. All rights reserved.